arXiv:1404.4933v2 [astro-ph.HE] 1 May 2014

A milliparsec supermassive black hole binary candidate in the galaxy SDSS J120136.02+300305.5

F.K. Liu[1,2], Shuo Li[3,1], and S. Komossa[4,5]

ABSTRACT

Galaxy mergers play a key role in the evolution of galaxies and the growth of their central supermassive black holes (SMBHs). A search for (active) SMBH binaries (SMBHBs) at the centers of the merger remnants is currently ongoing. Perhaps the greatest challenge is to identify the *inactive* SMBHBs, which might be the most abundant, but are also the most difficult to identify. Liu et al. predicted characteristic drops in the light curves of tidal disruption events (TDEs), caused by the presence of a secondary SMBH. Here, we apply that model to the light curve of the optically inactive galaxy SDSS J120136.02+300305.5, which was identified as a candidate TDE with *XMM-Newton*. We show that the deep dips in its evolving X-ray light curve can be well explained by the presence of a SMBHB at its core. A SMBHB model with a mass of the primary of $M_{\rm BH} = 10^7 M_\odot$, a mass ratio $q \simeq 0.08$, and a semimajor axis $a_{\rm b} \simeq 0.6\,$mpc is in good agreement with the observations. Given that primary mass, introducing an orbital eccentricity is needed, with $e_{\rm b} \simeq 0.3$. Alternatively, a lower mass primary of $M_{\rm BH} = 10^6 M_\odot$ in a circular orbit fits the light curve well. Tight binaries like this one, which have already overcome the "final parsec problem," are prime sources of gravitational wave radiation once the two SMBHs coalesce. Future transient surveys, which will detect TDEs in large numbers, will place tight constraints on the SMBHB fraction in otherwise non-active galaxies.

Subject headings: accretion, accretion disks – black hole physics – galaxies: active – galaxies: individual (SDSS J120136.02+300305.5) – gravitational waves – X-rays: galaxies

[1]Department of Astronomy, Peking University, Beijing 100871, China; *fkliu@pku.edu.cn*

[2]Kavli Institute for Astronomy and Astrophysics, Peking University, Beijing 100871, China

[3]National Astronomical Observatories, Chinese Academy of Sciences, 100012 Beijing, China

[4]Max-Planck-Institut für Radioastronomie, Auf dem Hügel 69, 53121 Bonn, Germany

[5]Kavli Institute for Theoretical Physics, Santa Barbara, CA 93106, USA

1. Introduction

During the hierarchical formation of galaxies, merging galaxies quickly bring two supermassive black holes (SMBHs) into their center, forming a hard SMBH binary (SMBHB) at parsec scale (Begelman et al. 1980; Quinlan 1996; Volonteri et al. 2003; Mayer et al. 2007; Tanaka & Haiman 2009; Kulkarni & Loeb 2012; Kulier et al. 2013). Further evolution of hard SMBHBs depends very much on the detailed nuclear structures. A hard SMBHB may stall at the parsec scale for a timescale longer than the Hubble time in the spherical and isotropic galactic nuclei (Begelman et al. 1980), but can be driven to the strong gravitational wave (GW) regime at milliparsec scale by efficient stellar dynamical processes in non-spherical, anisotropic, and/or rotating nuclear clusters (Merritt & Poon 2004; Berczik et al. 2006; Perets et al. 2007; Preto et al. 2011), or by hydrodynamic processes in massive gas disks (Gould & Rix 2000; Kocsis et al. 2012; Colpi & Dotti 2011, and references therein). If the orbits of SMBHBs could be highly eccentric (Armitage & Natarajan 2005; Berczik et al. 2006; Preto et al. 2011; Iwasawa et al. 2011; Sesana et al. 2011; Chen et al. 2011), the strong GW regime may extend far out and the SMBHBs can quickly evolve to the GW regime. The SMBHBs in the strong GW regime coalesce within a Hubble time. They are the primary targets for the proposed *Laser Interferometer Space Antenna* (*eLISA*) and ongoing Pulsar Timing Arrays (PTAs).

A few observations of SMBHBs in gaseous systems have been reported, ranging from spatially resolved binary active galactic nuclei (AGNs; e.g., Komossa et al. 2003; Rodriguez et al. 2006; Green et al. 2010; Liu et al. 2010; Fabbiano et al. 2011), to candidate un-resolved binary systems. The observational evidence for the latter is based on double-peaked broad emission lines in quasars and their variability (e.g., Tsalmantza et al. 2011; Ju et al. 2013; Shen et al. 2013); characteristic spatial structures in radio jets (e.g., Begelman et al. 1980; Conway & Wrobel 1995; Liu & Chen 2007; Roland et al. 2008; Britzen et al. 2012); quasi-periodic outbursts in some blazars (e.g., Sillanpaa et al. 1988; Liu et al. 1995, 1997, 2006; Liu & Wu 2002; Qian et al. 2007; Valtonen et al. 2011, and references therein); and swift jet reorientation in X-shaped radio galaxies (Liu 2004). Further, some candidate systems of coalesced SMBHBs have been identified, based on double-double radio galaxies that show an interruption and recurrence of jet formation (Liu et al. 2003), or based on evidence for recoiled SMBHs (e.g., Komossa et al. 2008a; Liu et al. 2012; Civano et al. 2012). All the observational evidence for SMBHBs in AGNs is consistent with the scenario of rapid migration of SMBHBs within massive gas disks.

However, most SMBHBs may form quiescently either in gas-poor or minor galaxy mergers without driving AGN activities. The high frequency of minor and gas-poor galaxy mergers is important in the formation and evolution of both late type and massive elliptical galaxies

(e.g., van Dokkum et al. 2010; Naab et al. 2009; McWilliams et al. 2012), therefore it is essential to understand the evolution of SMBHBs in quiescent galaxies, not only for the GW detections with *LISA* and PTA, but also to test the galaxy formation and evolution models. It is a challenge to detect dormant SMBHBs and observationally constrain their evolution in galactic nuclei. A dormant SMBH can be investigated observationally when it tidally disrupts stars passing by and becomes a transient AGN (Hills 1975; Luminet 1985; Rees 1988; Phinney 1989; Lodato et al. 2009). More than 20 candidates for stellar tidal disruptions (TDEs) by SMBHs have been reported in wavebands from γ-ray and X-ray through UV and optical to radio frequencies ((e.g., Komossa & Bade 1999; Komossa 2002; Komossa et al. 2008b; Gezari et al. 2008, 2012; Zauderer et al. 2011; Bloom et al. 2011; Burrows et al. 2011; Saxton et al. 2012b); (see Komossa 2012, for a review)). Recently, it was suggested that dormant SMBHBs in non-active galaxies could also be investigated when one of the SMBHs tidally disrupted a star, because SMBHBs can give some key imprints on the event rates, locations, and the environment in the galactic nuclei, light curves, and spectra of tidal flares (Ivanov et al. 2005; Komossa & Merritt 2008; Chen et al. 2008, 2009, 2011; Liu et al. 2009; Wegg & Nate Bode 2011; Stone & Loeb 2011, 2012b; Li et al. 2012; Chen & Liu 2013; Liu & Chen 2013). SMBHBs can dramatically change the tidal disruption rates of stars in galactic nuclei. Our investigations showed that stellar tidal disruption rates by ultra-compact SMBHBs, particularly in the GW dominated regime, are at least one order of magnitude lower (Chen et al. 2008), while those by bound (but not-hard) SMBHBs (Chen et al. 2009, 2011) or dual SMBHs in merging galaxies (Liu & Chen 2013) can be up to three orders of magnitudes higher than the estimated tidal disruption rates by single SMBHs in isolated galaxies (Wang & Merritt 2004). However, despite the significant difference in the tidal disruption rates, the separate contributions of stellar tidal disruptions by single, bound and hard binaries, and dual SMBHs to the total stellar disruption events during cosmic time are comparable to one another (Liu & Chen 2013), implying that some of the observed tidal disruption flares are probably from SMBHB systems. Numerical and analytic computations indicated that the stellar tidal disruption flares in SMBHB systems would show temporary interruptions and recurrences. The interruptions are due to the perturbation of the companion SMBH on the plasma streams of the tidally disrupted star (Liu et al. 2009, LLC09 hereafter). This is one of the key signatures for SMBHBs in galactic nuclei.

In this paper, we report the first candidate for a SMBHB in a quiescent galaxy. The galaxy SDSS J120136.02+300305.5 (SDSS J1201+30 hereafter) at redshift $z = 0.146$ was observed to be at outburst in X-rays with *XMM-Newton*, during the slew-survey observation on 2010 June 10, most probably due to the tidal disruption of a star by a SMBH at its center (Saxton et al. 2012b, S2012 hereafter). Follow-up observations in X-rays with the *Swift* and *XMM-Newton* space telescopes made by S2012 showed that the X-ray flux of the flare is, on

average, consistent with a $t^{-5/3}$ power law, as predicted by the canonical fallback model for tidal disruption (Rees 1988; Evans & Kochanek 1989). Superposed on this overall decline are rapid, strong dips in the X-ray flux. No absorption and no radio jet was detected in the observations. In particular, the light curve showed that SDSS J1201+30 decayed in the X-ray flux by more than about 50 times within seven days and became completely invisible to *Swift* between 27 and 48 days after discovery. Then, it recurred to follow the original power-law decay from 2010 October 24 to December 23. Here, we will show that all the striking features in the light curve of the event are challenging to understand by the TDE model in the presence of a single SMBH, but are fully consistent with the key predictions of the model for stellar tidal disruption in a SMBHB system, given by LLC09. Applying the binary black hole model for tidal disruption to SDSS J1201+30 and using the observations, we constrain well the parameters of the SMBHB system despite the gaps in the light curve coverage.

This paper is organized as follows. In Section 2, we introduce the fallback model for tidal disruptions of stars by SMBHs and give some general constraints on the model parameters for SDSS J1201+30, based on the observations given by S2012. In Section 3, we briefly describe the model for stellar tidal disruption in a SMBHB system (Section 3.1) and present the numerical results of employing the binary black hole model to SDSS J1201+30 in Section 3.2. We show that the observed light curve in X-rays can be well reproduced by a simple SMBHB model. In particular, the question of whether SMBHB orbits show eccentricity is important, both for the evolution of SMBHBs in galactic nuclei and the detection of GW radiation. We explore the effect of the orbital eccentricity of SMBHBs on the light curves, and show that the orbit of the SMBHB in SDSS J1201+30 must be elliptical, if the central black hole has a mass $\sim 10^7 M_\odot$ in Section 3.3. After critically investigating the alternatives in Section 4.1, we provide our discussion of the orbital parameters of the SMBHB system in SDSS J1201+30 in Section 4.2, the GW emission of the SMBHB system in Section 4.3, and the frequency of SMBHBs among known TDEs in Section 4.4. Throughout the paper, we assume a ΛCDM cosmology with parameters $H_0 = 70\,\mathrm{km\ s^{-1}\ Mpc^{-1}}$, $\Omega_\Lambda = 0.73$, and $\Omega_M = 0.27$.

2. Stellar tidal disruption in SDSS J1201+30

A star of mass M_* and radius R_* is tidally disrupted, if it passes by a SMBH with mass $M_{\rm BH}$ at a distance less than the tidal radius

$$r_{\rm t} \simeq R_* (\mu^2 M_{\rm BH}/M_*)^{1/3} \tag{1}$$

(Hills 1975; Rees 1988), where μ is of order unity. Because μ is degenerate with the other model parameters and cannot be constrained independently, we adopt $\mu = 1$ for simplicity.

When a star is tidally disrupted, the stellar plasma is redistributed in the specific energy E ranging from $E_{\rm b}-\Delta E$ to $E_{\rm b}+\Delta E$, where $E_{\rm b}$ is the total energy of the star before disruption and ΔE is the maximum specific energy obtained by the stellar plasma at disruption. If the star is bound to the SMBH, the total energy is $E_{\rm b}=-GM_{\rm BH}/(2a_*)$ with a_* the orbital semimajor axis of the bound star; while the total energy is $E_{\rm b}\sim\frac{1}{2}\sigma_*^2$ with σ_* the stellar velocity dispersion if the star is from the region around the influence radius of the SMBH. The maximum specific energy is

$$\Delta E\simeq kGM_{\rm BH}R_*/r_{\rm p}^2, \tag{2}$$

where G is the Newtonian gravitational constant, $r_{\rm p}$ is the orbital pericenter of the star, and $1\leq k\leq 3$ is a parameter depending on the spin of the star at disruption (Rees 1988; Li et al. 2002). If the tidal spin-up of the star is negligible $k=1$, while $k=3$ for a star being maximally spun up to break-up angular velocity. The spin-up of the star depends on the penetration factor $\beta\equiv r_{\rm t}/r_{\rm p}$. For a tidal disruption with $\beta\gtrsim 1$ as in SDSS J1201+30 (see discussions below) and because k is degenerate with β, we take $k=2.5$ as fiducial value. For a tidal disruption of penetration factor β, Equation (2) becomes

$$\Delta E\simeq\frac{kGM_{\rm BH}R_*}{r_{\rm t}^2}\times\beta^l, \tag{3}$$

where $l=2$. Equation (3) suggests a strong dependence of ΔE on β. Recent analytical and numerical calculations indicated, however, that ΔE might be nearly independent of β with $l\approx 0$, because ΔE is determined mostly by the conditions of the disrupted star around the tidal radius (Guillochon & Ramirez-Ruiz 2013; Stone et al. 2013; Hayasaki et al. 2013). In order to study the effects of different dependencies of ΔE on β, we also did calculations for $l=0$ (see Section 4.2 and Figure 1). The results show that our conclusions do not change with the relationship of ΔE and β. Thus, we use $l=2$ as the fiducial value throughout the paper, except when noticed otherwise.

The initial total energy of the star $E_{\rm b}$ is usually assumed to be negligible in the literature (except, e.g., Hayasaki et al. 2013) because stars approaching from the SMBH influence radius dominate the TDEs in single SMBH systems with spherical isotropic distributions of stars in the galactic nuclei (e.g., Magorrian & Tremaine 1999; Wang & Merritt 2004). However, the tidal disruptions are overwhelmed by the bound stars inside the SMBH sphere of influence due to either the scattering of the massive companion in SMBHB systems (Chen et al. 2009, 2011), or the chaotic orbits of stars in the galactic nuclei with triaxiality (e.g., Vasiliev & Merritt 2013; Liu & Chen 2013) and thus the total (binding) energy of stars is not necessary small. If the total energy of the bound stars has $|E_{\rm b}|\gtrsim\Delta E$, or an orbital

semi-major axis

$$a_* \lesssim a_{\rm cr} \simeq 1177.6 k^{-1} \beta^{-l} M_6^{-1/3} r_{\rm g} r_* m_*^{-2/3} \simeq 471 \left(\frac{k}{2.5}\right)^{-1} \beta^{-l} M_6^{-1/3} r_{\rm g} r_* m_*^{-2/3} \quad (4)$$

(where $r_{\rm g}$ is the Schwarzschild radius of the black hole, and $M_6 = M_{\rm BH}/10^6 M_\odot$ with $M_\odot$ the solar mass, $m_* = M_*/M_\odot$, and $r_* = R_*/R_\odot$ with $R_\odot$ the solar radius), the tidal disruption and the light curves of tidal flares are significantly different from the predictions by the canonical fallback model for unbound stars (Hayasaki et al. 2013). This is then inconsistent with the observations of SDSS J1201+30. For typical nuclear star clusters around SMBHs in the galactic nuclei, the fraction of stars with $a_* \lesssim a_{\rm cr}$ is negligible. Therefore, we assume $a_* \gg a_{\rm cr}$ or $|E_{\rm b}| \ll \Delta E$ and neglect $|E_{\rm b}|$ in the discussions of the TDE in SDSS J1201+30 from now on. However, this does not imply that the star is necessary from the influence radius of the SMBH.

The observations of the tidal flare in SDSS J1201+30 are consistent with the predictions of the canonical fallback model for stellar tidal disruption. In the canonical fallback model, the stellar plasma after tidal disruption distributes evenly in specific energy E between $-\Delta E$ and ΔE. Therefore about half of the stellar plasma gains energy and is ejected away from the system, while the other half loses energy and becomes bound to the SMBH. The bound stellar plasma follows Keplerian orbits with extremely high eccentricities and falls back to the pericenter at a mass rate

$$\dot{M}(t) \simeq \frac{M_*}{3t_{\rm min}} \left(\frac{t - T_{\rm D}}{t_{\rm min}}\right)^{-5/3} \text{ for } t \geq {\rm T_D} + {\rm t_{min}} \quad (5)$$

(Rees 1988; Evans & Kochanek 1989; Lodato et al. 2009), where $T_{\rm D} = 0$ is the epoch of disruption and $t_{\rm min}$ is the return time of the most bound stellar debris to the pericenter

$$\begin{aligned} t_{\rm min} &\simeq 2\pi G M_{\rm BH} (2\Delta E)^{-3/2} \simeq 41.0 \text{ days} \times k^{-3/2} \beta^{-3l/2} M_6^{1/2} r_*^{3/2} m_*^{-1} \\ &\simeq 10.4 \text{days} \times \left(\frac{k}{2.5}\right)^{-3/2} \beta^{-3l/2} M_6^{1/2} r_*^{3/2} m_*^{-1}. \end{aligned} \quad (6)$$

Equation (6) implies that $t_{\rm min}$ strongly depends on β, a parameter that cannot be given a priori. We take β as a free parameter and determine it observationally. Thus, we consider only the tidal disruption of solar-type stars and all the uncertainties are absorbed into β. After the bound stellar debris falls back to pericenter, it quickly circularizes at radius $r_{\rm c} \simeq 2r_p$ due to strong shocks between incoming and outgoing stellar plasma streams, leading to accretion onto the SMBH (Rees 1988; Phinney 1989; Ulmer 1999). Numerical simulations suggest that the accretion rate may peak at $t_{\rm peak} \sim 1.5 t_{\rm min}$ instead of time $t_{\rm min}$ as in Equation (5) (Evans & Kochanek 1989; Lodato et al. 2009). Equation (5) shows that the SMBH accretes

at rates larger than the Eddington accretion rate $\dot{M}_{\rm Edd} = L_{\rm Edd}/0.1c^2$ with the Eddington luminosity $L_{\rm Edd} = 1.25 \times 10^{44} M_6 \,{\rm erg\ s^{-1}}$, and c the speed of light, until a time

$$\begin{aligned} t &> t_{\rm Edd} \simeq 776 \text{ days} \times k^{-3/5} \beta^{-3l/5} M_6^{-2/5} m_*^{1/5} r_*^{3/5} \\ &\simeq 448 \text{ days} \times \left(\frac{k}{2.5}\right)^{-3/5} \beta^{-3l/5} M_6^{-2/5} m_*^{1/5} r_*^{3/5}. \end{aligned} \quad (7)$$

For the SMBHs of mass $3 \times 10^5 M_\odot < M_{\rm BH} < 2 \times 10^7 M_\odot$ in SDSS J1201+30 (S2012), $t_{\rm Edd}$ is on the order of months to years, depending on the penetration factor β. After a time

$$\begin{aligned} t &> t_{\rm ADAF} \simeq 33.7 \text{ yr} \times k^{-3/5} \beta^{-3l/5} M_6^{-2/5} \dot{m}_{-2}^{-3/5} m_*^{1/5} r_*^{3/5} \\ &\simeq 19.5 \text{ yr} \times \left(\frac{k}{2.5}\right)^{-3/5} \beta^{-3l/5} M_6^{-2/5} m_*^{1/5} r_*^{3/5} \dot{m}_{-2}^{-3/5} \end{aligned} \quad (8)$$

with $\dot{m}_{-2} = \dot{m}/0.01$, the accretion rate $\dot{m} = \dot{M}/\dot{M}_{\rm Edd}$ becomes less than 0.01 and the accretion mode probably becomes advection dominated (Narayan & Yi 1995). For a period of order of years, in which we are interested here, we have $\dot{m} > 0.01$ at high-states, and thus do not consider the change of accretion mode from radiatively efficient to inefficient.

To relate the fallback rates of stellar plasma to the observed X-ray flux in the 0.2-2 keV band, we need to know the ratio of the X-ray and bolometric luminosity, the transfer efficiency of matter to radiation, the fraction of the advected and photon-trapped energy into the SMBH, the fraction of the disk outflow to the total matter, the contribution and absorption of the disk corona, the amount of reflection, and the disk orientation. Because most of the processes cannot be determined from first principles, we simply adopt

$$L_X = f_{\rm x} \dot{M} c^2, \quad (9)$$

with $f_{\rm x}$ a free parameter to be fixed observationally. We assume $f_{\rm x}$ to be constant for the period we are interested in, and expect that this is a good assumption (e.g., Tanaka 2013). From Equations (5) and (9) and the data in Table 1 of S2012, we find that the tidal disruption happened about 11.8 days in the observer frame or $t_1 \simeq 10.3\,$days in the object rest frame before the first detection on 2010 June 10. To obtain t_1, we have used all the detections of SDSS J1201+30 given in Table 1 of S2012 except the observation on 2010 November 23 which was strongly affected by radiation. Because $f_{\rm x}$ in Equation (9) and $t_{\rm min}$ in Equation (5) are degenerate and cannot be determined independently by fitting the observational data, we can give only an upper limit to $t_{\rm min}$ as $t_{\rm min} \leq 10.3\,$days. If $l = 2$, from Equation (6) we have

$$\beta \simeq \left(\frac{t_{\rm min}}{41.0{\rm days}}\right)^{-1/3} \times k^{-1/2} M_6^{1/6} r_*^{1/2} m_*^{-1/3} \gtrsim 1.0 \left(\frac{k}{2.5}\right)^{-1/2} M_6^{1/6} r_*^{1/2} m_*^{-1/3}. \quad (10)$$

Thus the tidal disruption of the star in SDSS J1201+30 should occur inside the tidal radius with $\beta \gtrsim 1$. For $l = 0$, ΔE is independent of β, which gives a constraint on k alternatively

$$k \simeq \left(\frac{t_{\rm min}}{41.0{\rm days}}\right)^{-2/3} \times M_6^{1/3} r_* m_*^{-2/3} \gtrsim 2.5 M_6^{1/3} r_* m_*^{-2/3}. \quad (11)$$

The above analyses were carried out in Newtonian gravity. However, the disrupted star has a pericenter $r_{\rm p} = \beta^{-1} r_{\rm t} \simeq 12 M_6^{-2/3} (\beta/2)^{-1} r_{\rm g}$ and general relativity (GR) effects are important for a SMBH with mass $M_{\rm BH} \gtrsim 10^6 M_\odot$. To take the GR effect into account, we use the pseudo-Newtonian potential $\phi = GM_{\rm BH}/(r - r_{\rm g})$ (Paczyński & Wiita 1980) in our numerical simulations. Thus, Equation (2) is rewritten

$$\Delta E \simeq \frac{kGM_{\rm BH}}{1 - r_{\rm g}/r_{\rm p}} \frac{R_*}{r_{\rm p}^2} = \frac{kGM_{\rm BH}}{1 - \beta^{l/2} r_{\rm g}/r_{\rm t}} \frac{R_*}{r_{\rm t}^2} \beta^l. \quad (12)$$

With a larger maximum specific energy ΔE, Equation (6) gives a smaller $t_{\rm min}$, leading to a larger β and stronger GR effects.

3. A SMBHB system in SDSS J1201+30

3.1. SMBHB Model and Dynamic Evolution of the Accretion Disk

When SDSS J1201+30 becomes invisible to *Swift* during 2010 July 7 and July 28, the flux in X-rays decreases by more than 47 times within seven days from the last detection of 2010 June 30. Although the present observations can give only upper limits to the decay timescale with $\Delta t_{\rm dc} < 7$ days, and to the duration of being invisible in X-rays with 21 days $\leq \Delta t_{\rm in} \leq 116$ days, due to gaps in the observed light curve, we still have $\Delta t_{\rm dc} \ll \Delta t_{\rm in}$ and can give severe constraints on the possible models for the origin of the intermittence of the tidal flare. Here we explore in detail the SMBHB model as suggested by LLC09, and give a discussion on alternatives in Section 4.1.

In the SMBHB model (LLC09), the orbits of the less-bound and unbound stellar plasma change due to the strong perturbation by a massive object at a distance of several hundreds of Schwarzschild radii. Then, a significant fraction of the stellar plasma cannot fall back to form an accretion disk and to fuel the SMBH, leading to an intermittence of accretion onto the SMBH, and thus of the tidal flare. Because the massive perturber must be compact in order for it to survive the tidal force of the central SMBH, it is most probably a second SMBH. Before we numerically show how well the observations of SDSS J1201+30 can be reproduced by the theoretical light curves predicted by the SMBHB model in the Section 3.2, we first briefly introduce and discuss the merits of the SMBHB model.

After a star is tidally disrupted by a SMBH, the viscous interaction among the stellar plasma is negligible and the plasma fluid elements move ballistically with Keplerian orbits before they fall back to the pericenter and circularize because of strong shocks among the stellar tidal plasma (Evans & Kochanek 1989). For the ultra-bound fluid elements of Keplerian orbits with semi-major axis, much less than that of the SMBHB (hierarchical triple systems), the orbits of the fluid elements evolve secularly under the perturbation of the secondary SMBH on the Kozai-Lidov time scale (Kozai 1962; Lidov 1962), which is much larger than the Keplerian periods of the stellar fluid elements. The orbital angular momentum change, within one Keplerian period of the fluid elements, due to the torque caused by the quadrupole force of the secondary is

$$\delta J_{\rm fl} \sim \frac{3}{4}\frac{GM_2 a_{\rm fl}}{a_{\rm b}^3} a_{\rm fl} 2\pi \left(\frac{a_{\rm fl}^3}{GM_1}\right)^{1/2}, \tag{13}$$

where $a_{\rm fl}$ and $a_{\rm b}$ are, respectively, the semi-major axis of the fluid elements and the SMBHB. Because the relative change of the orbital angular momentum of the fluid elements

$$\begin{aligned}\frac{\delta J_{\rm fl}}{J_{\rm fl}} &\sim \frac{3\pi}{2}\frac{q(GM_1 a_{\rm fl})^{1/2}}{(GM_1 2r_{\rm p})^{1/2}}\left(\frac{a_{\rm fl}}{a_{\rm b}}\right)^3 \\ &\sim 2.2\times 10^{-3}\beta^{1/2} q_{-1}\left(\frac{10a_{\rm fl}}{a_{\rm b}}\right)^{7/2}\left(\frac{a_{\rm b}}{10^{-3}\,{\rm pc}}\right)^{1/2} m_6^{-1/6} r_*^{-1/2} m_*^{1/6}\end{aligned} \tag{14}$$

is very small, the fluid elements must fall back to the pericenter and accrete onto the SMBH as in a single SMBH system. In Equation (14), $q = M_2/M_1 = 0.1q_{-1}$ is the ratio of masses of the secondary and primary SMBHs.

However, when the fluid elements are less bound with semi-major axes $a_{\rm fl} \gtrsim a_{\rm b}/3$, the analytical and numerical simulations show that the orbits of the fluid elements become chaotic and change significantly on a Keplerian timescale (Mardling & Aarseth 2001; Liu et al. 2009) due to the nonlinear overlap of the multiple resonances (Mardling 2007). From Equation (14), we obtain the relative change of the orbital angular momentum of the fluid elements with $a_{\rm fl} \sim a_{\rm b}$ on Keplerian time

$$\frac{\delta J_{\rm fl}}{J_{\rm fl}} \sim 7.1\beta^{1/2} q_{-1}\left(\frac{a_{\rm fl}}{a_{\rm b}}\right)^{7/2}\left(\frac{a_{\rm b}}{10^{-3}\,{\rm pc}}\right)^{1/2} m_6^{-1/6} r_*^{-1/2} m_*^{1/6}, \tag{15}$$

and the fluid elements would move with chaotic orbits of pericenter $r_{\rm p,fl} \sim 110 r_{\rm p}$, which is much larger than the pericenter $r_{\rm p}$ at disruption. Therefore, the fluid elements move with chaotic orbits significantly different from one another. They neither fall back to the pericenter at disruption, nor cross each other to form shocks and accretion. The transition radius, or corresponding Keplerian time $T_{\rm tr}$ of the fluid elements from secular to chaotic orbits, depends

critically on the orbital parameters of the stars and also of the SMBHB system, but $T_{\rm tr}$ can relate to the SMBHB orbit period, with $T_{\rm tr} = \eta T_{\rm b}$ (LLC09). The parameter η is a strong function of the orbital parameters of the star, but is insensitive to the SMBH masses (LLC09). Statistically, η is in the range $0.15 \lesssim \eta \lesssim 0.5$ with a mean value $\eta \sim 0.25$ for a SMBHB system with eccentricity $e_{\rm b} = 0$. Therefore, if η is known, one can determine the orbital parameters of the star and SMBHB system. Taking into account that the first detection of the tidal flare in SDSS J1201+30 is about 11.8 days after the tidal disruption of the star and that the X-ray flux becomes invisible at a time between 20 and 27 days after discovery, we determine that the observed truncation time is 31.8 days $\leq T_{\rm tr,obs} \leq$ 38.8 days in the observer frame, or 27.7 days $\leq T_{\rm tr} \leq$ 33.9 days in the object rest frame.

When the stellar plasma stops falling back and fueling the accretion disk of the outer radius $r_{\rm d} \approx r_{\rm c}$, the accretion disk evolves dynamically on the viscous timescale at $r \approx r_{\rm d}$

$$\begin{aligned} t_{\nu,{\rm d}} &= \frac{2}{3}\frac{r_{\rm d}^2}{\nu(r_{\rm d})} \simeq \frac{2}{3}\alpha^{-1}\left(\frac{r_{\rm d}^3}{GM_{\rm BH}}\right)^{1/2}\left(\frac{H}{r}\right)^{-2}_{\rm r=r_d} \\ &\simeq 0.12 \text{ days} \times \alpha_{-1}^{-1}\left(\frac{\beta}{2}\right)^{-3/2}\left(\frac{H}{r}\right)^{-2}_{\rm r=r_d} r_*^{3/2} m_*^{-1/2}, \end{aligned} \tag{16}$$

where $\alpha = 0.1\alpha_{-1}$ is the disc viscosity coefficient and H is the scaleheight of the disk with $H \simeq r$ for the accretion rate $\dot{m} \gtrsim 0.3\dot{M}_{\rm Edd}$ (Shakura & Sunyaev 1973; Abramowicz et al. 1988; Strubbe & Quataert 2009). Equation (16) suggests that $t_{\nu,{\rm d}}$ is independent of the mass of the central SMBH. For SDSS J1201+30, Equations (5) and (6) suggest that the accretion rate $\dot{M}$ is much larger than $\dot{M}_{\rm Edd}$ when the source was absent from the *Swift* observation on 2010 July 7, or 33.9 days after tidal disruption. Therefore, the accretion disk in SDSS J1201+30 dynamically evolves on the viscous timescale $t_{\nu,{\rm d}} \sim 0.12$ days for a typical viscous parameter $\alpha = 0.1$. This is about 60 times less than the time interval between the last detection on 2010 June 30 and the first absence from the *Swift* observation on 2010 July 7 (S2012).

For the dynamic evolution of the accretion disk without the fueling of stellar plasma, here we construct a simple model to describe it, by assuming that ν is only a function of radius with $\nu \propto r^n$. For the physical model of an accretion disk in tidal disruption as proposed by Strubbe & Quataert (2009), a kinematical viscosity $\nu = \alpha c_s H \propto r^n$ with $n = 1/2$ is a good approximation and adopted in the model. For an accretion disk with $\nu \propto r^n$, the dynamic evolution can be solved analytically and the surface density Σ can be given by making use of a Green's function $G(r,t)$

$$\Sigma(r,t) = \int_{r_{\rm in}}^{r_{\rm d}} G(r,R,t)\Sigma(R,t=t_{\rm tr})dR, \tag{17}$$

(Lynden-Bell & Pringle 1974; Tanaka 2011), where $\Sigma(R, t = t_{tr})$ is the initial disk surface density when the stellar plasma stops fueling the accretion disk at $t = t_{\rm tr}$, $r_{\rm in}$ ($r_{\rm in} \simeq 3r_{\rm g}$ for a Schwarzschild black hole) is the inner radius of the accretion disk, and the Green's function $G(r, R, t)$ is

$$G(r,R,t) \approx \frac{2-n}{\Gamma(j+1)}\left(\frac{r}{r_{\rm d}}\right)^{-n} r_{\rm d}^{-5/2} R^{3/2} \tau^{-1-j} \exp\left[-\frac{(r/r_{\rm d})^{2-n}+(R/r_{\rm d})^{2-n}}{\tau}\right] \quad (18)$$

for $t - t_{\rm tr} \gtrsim t_\nu(r_{\rm d})$. Here, $j = (4-2n)^{-1}$, $\tau = 2(2-n)^2(t-t_{\rm tr})/t_{\nu,{\rm d}}$, and $\Gamma(j)$ is the Gamma function. At the moment, when the stellar plasma stops fueling the accretion disk, the surface density is approximately

$$\Sigma(R, t = t_{\rm tr}) \approx \Sigma_{\rm d}\,(R/r_{\rm d})^{-n}, \quad \text{for} \quad r_{\rm in} \le R \le r_{\rm d} \quad (19)$$

where $\Sigma_{\rm d} \approx \dot{M}_0/(3\pi\nu(r_{\rm d}))$ and $\dot{M}_0$ is the accretion rate at time $t = t_{\rm tr}$. From Equations (17), (18), and (19), we have

$$\Sigma(r,t) \approx \frac{2(2-n)}{(5-2n)\Gamma(j+1)}\Sigma_{\rm d}\left(\frac{r}{r_{\rm d}}\right)^{-n}\left[2(2-n)^2\frac{(t-t_{\rm tr})}{t_{\nu,{\rm d}}}\right]^{-j-1}\left[1-\left(\frac{r_{\rm in}}{r_{\rm d}}\right)^{\frac{5}{2}-n}\right], \quad (20)$$

which gives an inward radial mass flow

$$\dot{M} = 6\pi r^{1/2}\frac{\partial}{\partial r}\left(\nu\Sigma r^{1/2}\right) \approx \frac{2(2-n)}{(5-2n)\Gamma(j+1)}\dot{M}_0\left[1-\left(\frac{r_{\rm in}}{r_{\rm d}}\right)^{\frac{5}{2}-n}\right]\left[2(2-n)^2\frac{(t-t_{\rm tr})}{t_{\nu,{\rm d}}}\right]^{-j-1} \quad (21)$$

for $(t - t_{\rm tr}) \gtrsim t_{\nu,{\rm d}}$. For a typical value $n = 1/2$, we have

$$\dot{M}(t - t_{\rm tr} \gtrsim t_{\nu,{\rm d}}) \approx 0.113\,\dot{M}_0\left[1-\left(\frac{r_{\rm in}}{r_{\rm d}}\right)^2\right]\left[\frac{t-t_{\rm tr}}{t_{\nu,{\rm d}}}\right]^{-4/3}. \quad (22)$$

Equation (22) shows that the accretion rate in SDSS J1201+30 decreases 50 times within about $3.7t_{\nu,{\rm d}} \sim 0.4 - 1$ days after the stellar plasma stops fueling the accretion disk. One has to notice that the accretion disk changes the accretion mode to advection dominated accretion flows (ADAFs) for $\dot{M} \lesssim 10^{-2}\dot{M}_{\rm Edd}$ (Narayan & Yi 1995) and our simple model cannot be applied to the transition. Because an ADAF is radiatively inefficient, it is expected that the object becomes even dimmer.

The numerical simulations by LLC09 suggested that after a time interval, the stellar plasma starts refueling the accretion disk and the tidal disruption flare recurs. The exact time when the tidal flare recurs depends on both the parameters of the star and the SMBHB system, but it is about at time $T_{\rm r} = \xi T_{\rm b}$ with ξ of order unity. Given the gaps in the

light curve of SDSS J1201+30 , the recurrence of the tidal flare can happen between 2010 July 28 and October 24, suggesting a recurrent time $T_{\rm r,obs}$ between 60 days and 148 days in the observer frame or $T_{\rm r}$ between 52 days and 129 days in the object rest frame. Therefore, the orbital period, $T_{\rm b}$ ($\sim T_{\rm r}$), of the SMBHB in SDSS J1201+30 is on order of, or less than, a few hundred days. The suggested orbital period of the SMBHB, together with 28 days $< T_{\rm tr} <$ 34 days, suggests $0.2 \lesssim \eta \lesssim 0.6$, which is consistent with the prediction of the SMBHB model. Whether and when the recurrent flare is interrupted again depends not only on the orbital parameters of the star and SMBH system, but also on the mass ratio and the total masses of the SMBHs, which have to be determined numerically (LLC09).

3.2. Numerical simulations and results

In Section 3.1, we showed that the observations of the tidal flare in SDSS J1201+30 are consistent over all with the predictions of the SMBHB model of LLC09. In this section, we numerically calculate the model light curves for the different parameters and quantitatively compare them one by one with the light curve of SDSS J1201+30 in X-rays. Given the sampling of the light curve of the tidal flare, we do not use the least-square method to get the best fit of the model predictions to the observations, but instead numerically explore the model parameter space to obtain the range of the parameters with which the SMBHB model can give theoretical light curves reasonably reproducing the observations of SDSS J1201+30.

In the simulations, for simplicity we assume that the disrupted star is a solar-type main-sequence star of parameter $k = 2.5$, and that the SMBHs is a Schwarzschild black hole, which is consistent with the suggestions given by the correlation of black hole spin and jet power (Narayan & McClintock 2012). In this section, we consider SMBHB systems of circular orbit with $e_{\rm b} = 0$, while the effects of the orbital eccentricity of the SMBHB are investigated in Section 3.3. The other parameters, both of the disrupted star and the SMBHB system, are explored and tested in a large range of values.

The method of the numerical simulations used in this work was described in detail in LLC09. Here we give only a summary and interested readers are referred to that paper. Because the interaction between the fluid elements is negligible before they return to the pericenter of the disrupted star and experience strong shocks because of the intersection and collision of the fluid elements with one another near pericenter, we can simulate the orbital evolution of the fluid elements with scattering experiments and calculate the fallback and accretion rate of the stellar plasma onto the central SMBH, by assuming that all the stellar plasma falling back to a radius of around $2r_{\rm p}$ or less is accreted. In each scattering experiment, the mass of the star is divided into fluid elements with specific energy $E_{\rm fl}$ and

constant pericenter $r_{\rm p}$, by assuming a constant distribution of mass in the specific energy in a range of $-\Delta E$ and ΔE, which is given by Equation (12) with $k = 2.5$. When the fluid elements moving in the pseudo-Newtonian potential return and pass by the central SMBH within a distance $2r_{\rm p}$, the calculation stops and the fluid element and the time are recorded, respectively, as accreted matter and accretion time. Otherwise, the calculation continues until time $4T_{\rm b}$ (the largest timescale in which we are interested) or the fluid element escapes from the system. The accretion rate of the stellar plasma is computed using the recorded fluid element masses and accretion time. We then compare the model accretion rate and the observations by adjusting the free parameter $f_{\rm x}$ in Equation (9). To reproduce the observations, we require a model light curve (1) to have an interruption between 2010 June 30 and July 6, one day before the first observation of absence on 2010 July 7; (2) that a recurrent flare begins between 2010 July 28 and October 24, and ends between 2010 December 13 and 2011 March 5; and (3) to have a second interruption during the period around 2011 April 1.

Because the SMBH masses cannot be determined uniquely in the SMBHB model by fitting the observations of the tidal flare, they have to be estimated separately and taken as input values in the simulations. Based on the relationship of black hole mass and bulge luminosity of the host galaxy, S2012 estimated a black hole mass in the range $3 \times 10^5 M_\odot < M_{\rm BH} < 2 \times 10^7 M_\odot$ with a higher value of $M_{\rm BH} \sim 10^7 M_\odot$ preferred. We have only done scattering experiments for three typical values of the mass of the primary SMBH, $M_{\rm BH} = 10^6 M_\odot$, $5 \times 10^6 M_\odot$, and $10^7 M_\odot$. For a given mass of the primary black hole, the mass of the secondary is calculated with the mass ratio q, which is determined by reproducing the observed light curve. The results of the numerical simulations show that the interruption time $T_{\rm tr}$, the recurrent time $T_{\rm r}$, and the duration of the recurrent flare strongly not only depend on the orbital parameters of the disrupted star at disruption, including (1) the penetration factor β, (2) the inclination angle θ between the orbital planes of the star and the SMBHB, and (3) the longitude of ascending node Ω and the argument of pericenter ω of the stellar orbits relative to the orbit plane of the SMBHBs. They also depend on the orbital period of the SMBHB, the SMBH masses, and the black hole mass ratio q. To obtain the possible model light curves consistent with the observations, in principle we have to do a large amount of high precision simulations to cover all the space of the seven model parameters, which would consume a large amount of computation resources and is prohibitive for present computing power. However, the discussions in Section 3.1 suggested that the orbital period of the SMBHB is of order hundred days, which could be taken as a good initial value of the orbital period $T_{\rm b}$ and used to reduce the computations. LLC09 suggested that, with a given orbital period of the SMBHB, the interruption time $T_{\rm tr}$ and the characters of recurrent flares depend sensitively on the stellar orbital parameters θ,

Ω, and ω, but less on the parameters of the SMBHB system. Therefore, we started the simulations from taking $T_{\rm b} \sim 135\,{\rm days}$ and $q \sim 0.1$ as initial values and carried out the simulations for different values of $\theta \in [0, \pi]$, $\Omega \in [0, 2\pi)$, and $\omega \in [0, 2\pi)$ with a resolution of 0.1π in all the parameter space to obtain the typical sets of parameter values giving model light curves closest to (but not necessary fully reproducing) the observations. After a large number of simulations, we found that the model light curves obtained with both $\theta \sim 0.3\pi$ and $\theta \sim 0.5\pi$ can give a reasonable fit to the observations, and the present observations of SDSS J1201+30 cannot tell which one is preferred. Those simulations with $\theta < 0.3\pi$ tend to give a longer duration for the first part of the light curve, which is inconsistent with the observed truncated light curve around 2010 July 7. For the simulations with $\theta > 0.5\pi$, most of the results cannot give a proper recurrence as observed in SDSS J1201+30 . Therefore, our results prefer a disrupted star with a prograde orbit relative to the SMBHB for SDSS J1201+30 . However, our model cannot entirely exclude a disrupted star with a retrograde orbit, because there are a few results with $\theta \gtrsim 0.5\pi$ still marginally consistent with the observation. Further observations with higher time resolution may help to solve the ambiguity. The simulation results suggest that the required values of the parameters of the SMBHB are nearly independent of the values of either $\theta \sim 0.3\pi$ or $\theta \sim 0.5\pi$, although the solutions for $\theta = 0.5\pi$ are fine tuning, in the sense that the solutions become significantly different from the observations for a small deviation of θ from $\theta = 0.5\pi$. Because we are mostly interested in the values of the parameters of the SMBHB system and the large gaps in the light curve do not warrant any fine tuning solution, we adopt the solutions of $\theta \sim 0.3\pi$. After $\theta \sim 0.3\pi$ is chosen, we obtain the corresponding values of the other orbital parameters of the star: $\Omega = 0.2\pi$ and $\omega = 1.5\pi$. Again, our test simulation results show that the values of the model parameters of the SMBHB system required to reproduce the observed light curve are nearly independent of the values of Ω and ω. Therefore, we will give the numerical simulation results for $\theta = 0.3\pi$, $\Omega = 0.2\pi$, and $\omega = 1.5\pi$. With the given values of θ, Ω, and ω, we have carried out the numerical simulations iteratively, starting from the initial values $T_{\rm b} = 135\,{\rm days}$, $q = 0.1$ and $\beta = 2$, for the penetration factor β between $1 \leq \beta \leq 6$, $1 \leq \beta \leq 3$ and $1 \leq \beta \leq 2.5$ and for the orbital period $T_{\rm b}$ between $130\,{\rm days} \leq T_{\rm b} \leq 160\,{\rm days}$, $135\,{\rm days} \leq T_{\rm b} \leq 170\,{\rm days}$, $120\,{\rm days} \leq T_{\rm b} \leq 200\,{\rm days}$, respectively, for $M_{\rm BH} = 10^6 M_\odot$, $M_{\rm BH} = 5 \times 10^6 M_\odot$ and $M_{\rm BH} = 10^7 M_\odot$, and the mass ratio q between $0.03 < q < 0.9$, in order to obtain all the model light curves fully consistent with the observations, including the positive detections and upper limits in X-ray flux.

We first carry out the numerical simulations for SMBHB systems with a primary black hole of mass $M_{\rm BH} = 10^6 M_\odot$. The top panel in Figure 1 gives two examples of the model light curve for a penetration factor $\beta = 3.0$ (solid red line) and $\beta = 3.5$ (dashed blue line), with $l = 2$, which can fully reproduce the X-ray observations of the tidal flare in SDSS

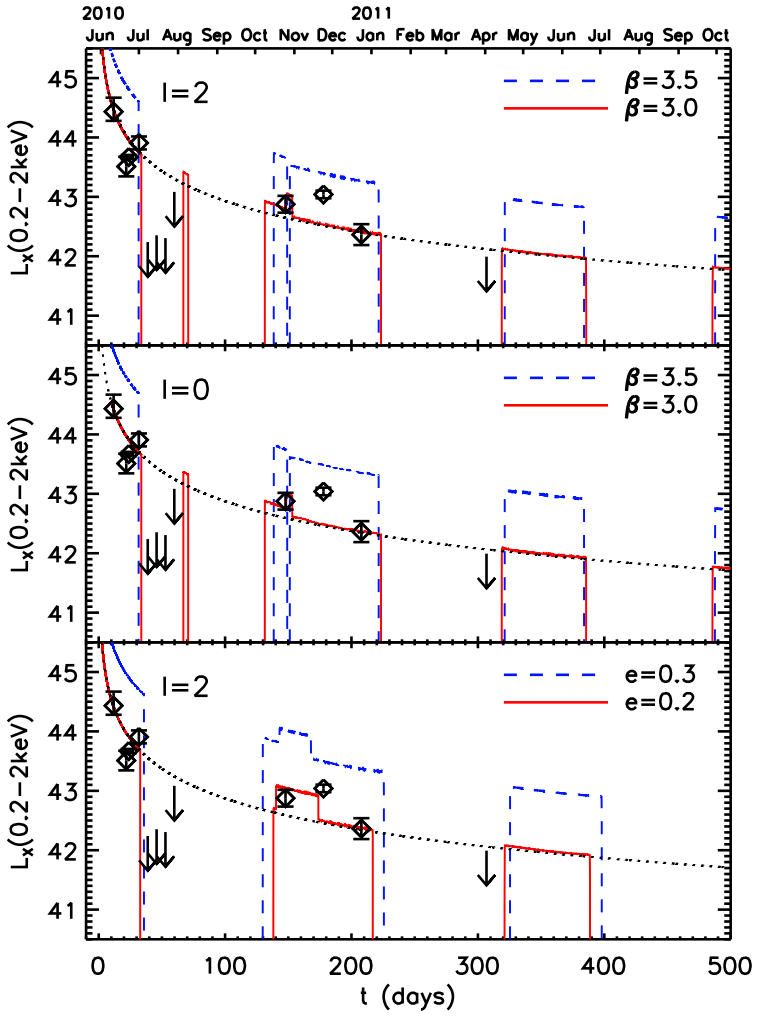

Fig. 1.— Simulated light curves in the observer frame for SDSS J1201+30 obtained with $M_{\rm BH} = 10^6 M_\odot$. Observational data from S2012 (open diamonds and arrows for upper limits) and a $t^{-5/3}$ power-law (dotted line) are overplotted. The top x-axis gives the dates of observation. In the simulations, $\theta = 0.3\pi$, $\Omega = 0.2\pi$, and $\omega = 1.5\pi$. Top panel: results for penetration factor $\beta = 3.0$ (solid red line) and $\beta = 3.5$ (dashed blue line, shifted upwards by 1 dex) with $l = 2$. For both simulations, $e_{\rm b} = 0$, $T_{\rm b} = 140\,$days, and $q = 0.1$. Middle panel: same as top panel while $l = 0$. The differences of the light curves between the top and middle panels are $t_{\rm min}$ and $f_{\rm x}$ (see text for details). The first interruption in the light curve for $\beta = 3.0$ appears on 2010 July 2, about two days after the last detection and five days before the first upper limit. Bottom panel: results for the elliptical binary orbits with $e_{\rm b} = 0.2$ (solid red line) and $e_{\rm b} = 0.3$ (dashed blue line, shifted upwards by 1 dex), with $l = 2$. For both simulations $\phi_{\rm b} = 1.7\pi$, $T_{\rm b} = 150\,$days, $q = 0.1$, and $\beta = 2.0$. The first interruption in the light curve for $e_{\rm b} = 0.2$ appears on 2010 July 4.

J1201+30. To obtain the model light curve in Figure 1, we have adopted a SMBHB with an orbital eccentricity $e_{\rm b} = 0$ and a period $T_{\rm b} \simeq 140\,{\rm days}$, and a black hole mass ratio $q \simeq 0.1$. To compare the theoretical light curve and the observations in the X-rays, we overplot the observational X-ray data and shift the theoretical light curve up and down in order to obtain a good fit by eyes, which gives a scaling factor in Equation (9), $f_{\rm x} = 0.004$. For a typical transfer efficiency of matter to radiation $\epsilon = 0.1$, this gives a total mass accreted $\Delta M_{\rm acc} \sim 0.02 M_\odot$, very small but consistent with the reported values for TDEs in the literature (e.g., Komossa 2002; Li et al. 2002; Komossa et al. 2004; Esquej et al. 2008; Gezari et al. 2009; Cappelluti et al. 2009; Maksym et al. 2010; Donato et al. 2014). We recall that a number of unknowns determines the precise amount of X-ray emission in the early evolution of TDEs and the unobserved EUV component may dominate the bolometric luminosity, as discussed in Section 2. Therefore the value we report here just serves as an order-of-magnitude estimate and lower limit. We notice that the orbital period of the SMBHB, $T_{\rm b} \simeq 140\,{\rm days}$, obtained by detailed numerical simulations, is consistent with the simple estimation given in Section 3.1. The period $T_{\rm b} \simeq 140\,{\rm days}$ together with the black hole mass ratio $q = 0.1$, suggests that the SMBHB in SDSS J1201+30 has an orbital radius $a_{\rm b} \simeq 0.26 M_6^{1/3}\,{\rm mpc} \simeq 2.8 \times 10^3 M_6^{-2/3} r_{\rm g}$. Figure 1 shows that the recurrent flares in the SMBHB model light curve fit the observations of SDSS J1201+30 in the X-rays better than a simple $t^{-5/3}$-power law decay, except for the observation on 2010 November 23, which was strongly affected by radiation (S2012).

For comparison, we re-do the simulations in Figure 1 with the same parameters, except $l = 0$. The results have been plotted in the middle panel of Figure 1. Comparing to the top panel, there are only small differences at the beginning of the light curve. Based on Equation (3), the energy dispersion for $l = 0$ is smaller than $l = 2$ when $\beta > 1$, which results in a larger $t_{\rm min}$. However, those changed $t_{\rm min}$ in Figure 1 are still consistent with the observation. Besides, as implied by Equations (5) and (9), since $\dot{M}(t) \propto t_{\rm min}^{2/3}$, a larger $t_{\rm min}$ will lead to a smaller $f_{\rm x}$. As a result, $f_{\rm x} = 0.0004$ for the middle panel of Figure 1, which is an order of magnitude lower than for the model of the top panel. As shown in the middle panel, however, ΔE is independent of β when $l = 0$, and the overall light curve is still impacted by β, because the truncation and recurrence of the light curve in the SMBHB system are sensitively depending on the size of the circularized accretion disk, which should be changed for a different β value.

From Figure 1, the first interruption in the model light curve for $\beta = 3.0$ happens at about time $T_{\rm tr,obs} = 34$ days after the tidal disruption of the star, or on 2010 July 2, which is about two days after the last detections on June 30 or five days before the first upper limit of the *Swift* observation on 2010 July 7. Equation (22) suggests a decay of the accretion rate by about a factor 600 within five days. This is consistent with the observation of a factor > 48 within seven days. We note that for such a large decrease of the accretion rate, the

simple dynamic model of the accretion disk may not be applicable anymore. The theoretical light curve for $\beta = 3.0$ suggests that the stellar plasma stops returning and fueling the accretion disk for a period $\Delta T_{\rm tr,obs} \approx 98$ days, intermingling with a flicker of accretion for about four days around 2010 August 7. The stellar plasma restarts fueling the accretion disk at about 131 days after the tidal disruption or about 16 days before the detection with *Swift* on 2010 October 24. After about 92 days, the recurrent tidal flare is interrupted again, at about 16 days after the last detection with *XMM-Newton* on 2010 December 23. This model predicts that the interrupted tidal flare will recur again later.

The results given in Figure 1 show that the observed X-ray light curve of SDSS J1201+30 can be fully reproduced by the theoretical light curve obtained with the typical model parameters $\theta = 0.3\pi$, $\Omega = 0.2\pi$, $\omega = 1.5\pi$, $\beta = 3.0$, $M_{\rm BH} = 10^6 M_\odot$, $q = 0.1$, $e_{\rm b} = 0$, and $T_{\rm b} = 140$ days. While our simulation results also show that the observed light curve can be well reproduced by the theoretical light curves obtained with model parameters in a broader range of values, namely, $1.2 \lesssim \beta \lesssim 5.0$, 132 days $\lesssim T_{\rm b} \lesssim 145$ days and $0.05 \lesssim q \lesssim 0.18$. The upper panel of Figure 1 also gives the theoretical light curve obtained with penetration factor $\beta = 3.5$ (dashed blue line). Values of the other model parameters are the same as for $\beta = 3.0$. Figure 1 shows that a small change of the penetration factor β from $\beta = 3.0$ to $\beta = 3.5$ would result in significant changes not only of the time and duration of interruption, but also of the variability of the recurrent flares. The simulation results show that the variations of the penetration factor β can significantly change the timescale $t_{\rm min}$, interruption and recurrent time, the duration of the recurrent flare, and the secondary recurrent time. In fact, all the key signatures in the light curves for SMBHBs strongly depend on complex combinations of the parameters β, $T_{\rm b}$, and q. This implies that the orbital parameters of the star and the SMBHB system, together with black hole mass ratio (except for the mass of the primary SMBH), can be determined observationally, when one can obtain very densely sampled TDE light curves in the future. A deeper exploration of the allowed values in parameter space is given in Section 4.2.

Because the mass of the primary BH in SDSS J1201+30 is loosely constrained by observations (approximately within the range $3 \times 10^5 M_\odot$ and $2 \times 10^7 M_\odot$), we have also carried out the numerical simulations for SMBHB systems with black hole mass $M_{\rm BH} = 5 \times 10^6 M_\odot$ and $M_{\rm BH} = 10^7 M_\odot$, and compare the model light curves with the X-ray observations of SDSS J1201+30 . Again, here we only consider SMBHB systems with circular orbit. The simulations are carried out for model parameters in the ranges $0.03 \leq q \leq 0.9$, $1 \leq \beta \leq 3$ and $1 \leq \beta \leq 2.5$, respectively, for $M_{\rm BH} = 5 \times 10^6 M_\odot$ and $M_{\rm BH} = 10^7 M_\odot$. The simulation results show that for a SMBHB system with $M_{\rm BH} = 5 \times 10^6 M_\odot$ and $e_{\rm b} = 0$ a set of fine-tuned values of model parameters can give theoretical light curves consistent with the observations. However, for a SMBHB system with $M_{\rm BH} = 10^7 M_\odot$ and $e_{\rm b} = 0$, no theoretical

light curve is found to be fully consistent with the observations, in the sense that either the predicted first interruption date is later than the first upper limit on July 7 or the predicted recurrent flares do not cover all the observations from 2010 October 24 to December 23. As a result, if the orbit of the SMBHB in SDSS J1201+30 is circular, the primary SMBH most probably has a mass $M_{\rm BH} \lesssim 5 \times 10^6 M_\odot$. Otherwise, if the SMBH has a mass $M_{\rm BH} \sim 10^7 M_\odot$ as preferred by the observations (S2012), the SMBHB is hardly circular, however, because of the limited coverage of the parameter space the present simulations cannot completely rule out the possibility that fine-tuning the model parameters might give solutions to the observational light curve. We will explore the effects of orbital eccentricity on the results in the next section.

3.3. Orbital eccentricity of the SMBHB system

The orbits of SMBHBs in galactic nuclei could be elliptical as suggested by some models for the formation and evolution of SMBHBs in galaxies (Armitage & Natarajan 2005; Berczik et al. 2006; Preto et al. 2011; Iwasawa et al. 2011; Sesana et al. 2011; Chen et al. 2011). Because the eccentricity of SMBHBs is of great importance in modeling the templates of gravitational waveforms, we now investigate if the observations of SDSS J1201+30 can give any constraint on the orbital eccentricity. For an elliptical orbit, in addition to the model parameters described in Section 3.2, we now have two more parameters, the eccentricity $e_{\rm b}$ and the initial phase $\phi_{\rm b}$ of the SMBHB orbit at the disruption of the star. In the simulations, $\phi_{\rm b}$ is set to be zero when the two SMBHs are at closest distance. We have carried out the scattering experiments by using the methods given in Section 3.2 and varying the eccentricity and initial orbital phase in the ranges of $0 \leq e_{\rm b} \leq 0.9$ and $0 \leq \phi_{\rm b} < 2\pi$, respectively. The simulation results show that both the time of interruption and recurrence, and the durations of the recurrent flares of the model light curves significantly change with $e_{\rm b}$ and $\phi_{\rm b}$. If the mass of the primary SMBH is $M_{\rm BH} = 10^6 M_\odot$, the observations of SDSS J1201+30 can be well reproduced with the model light curves obtained with the eccentricity $0 \leq e_{\rm b} \lesssim 0.5$ and initial orbital phase $1.3\pi \lesssim \phi_{\rm b} \lesssim 2\pi$. The bottom panel of Figure 1 gives two examples of model light curves for SDSS J1201+30 computed with $e_{\rm b} = 0.1$, $e_{\rm b} = 0.2$ and $l = 2$. The first interruption in the light curve for $e_{\rm b} = 0.2$ happens on 2010 July 4, about four days after the last detection and three days before the first upper limit on 2010 July 7. The recurrent fluxes in the model light curves fit the observations of SDSS J1201+30 better than a simple power-law decay. To obtain the light curves in the bottom panel of Figure 1, we have used the parameters $T_{\rm b} \simeq 150\,{\rm days}$ (or $a_{\rm b} \simeq 0.28\,{\rm mpc}$), $\phi_{\rm b} = 1.7\pi$ and $q = 0.1$ for the SMBHB system, and $\beta = 2.0$, $\theta = 0.3\pi$, $\Omega = 0.2\pi$, $\omega = 1.5\pi$ for the star. For $e_{\rm b} = 0.2$, the model light curves obtained with $0.05 \lesssim q \lesssim 0.15$, $1.2 \lesssim \beta \lesssim 4.7$ and $140\,{\rm days} \lesssim T_{\rm b} \lesssim 155\,{\rm days}$, can

fully reproduce the observations of SDSS J1201+30 . We notice that the values of θ, Ω, and ω used in the simulations are the same as for circular SMBHB systems. In fact, to reproduce the observed light curve of SDSS J1201+30 , we take $\theta = 0.3\pi$, $\Omega = 0.2\pi$, and $\omega = 1.5\pi$ in all the simulations for different eccentricities. However, we have to adopt different mass ratios and values of the SMBHB orbital parameters, because the interruption and recurrence in the model light curves depend on a complex combination of the parameters of the SMBHBs. In conclusion, the present observations of SDSS J1201+30 can constrain the eccentricity of the SMBHB only in the range $0 \leq e_{\rm b} \lesssim 0.5$, if the primary SMBH has a mass $10^6 M_\odot$.

For $M_{\rm BH} = 5 \times 10^6 M_\odot$, the simulation results show that the X-ray observations of SDSS J1201+30 can also be reproduced with model light curves obtained with binary eccentricity $0 \leq e_{\rm b} \lesssim 0.5$. For a SMBHB system with orbital eccentricities $e_{\rm b} \gtrsim 0.5$, no model light curve is able to reproduce the X-ray light curve of SDSS J1201+30 . For SMBHB systems with an even higher SMBH mass of the primary, of $M_{\rm BH} \sim 10^7 M_\odot$, our results show that we can obtain model light curves to reproduce the X-ray observations of SDSS J1201+30 if the orbit of the SMBHB is elliptical with eccentricity $0.1 \lesssim e_{\rm b} \lesssim 0.5$. If so, the SMBHB system in SDSS J1201+30 would have an orbital period $140\,{\rm days} \lesssim T_{\rm b} \lesssim 160\,{\rm days}$ and a black hole mass ratio $0.04 \lesssim q \lesssim 0.09$. The disrupted star would have a penetration factor $1.3 \lesssim \beta \lesssim 1.6$ at disruption. The orbital parameters then adopt the typical values: $\theta \simeq 0.3\pi$, $\Omega \simeq 0.2\pi$, $\omega \simeq 1.5\pi$, and $\phi_{\rm b} \simeq 1.5\pi$. Figure 2 gives the simulated light curves for SDSS J1201+30 by a SMBHB model with $M_{\rm BH} = 10^7 M_\odot$ and $e_{\rm b} = 0.3$. To obtain the light curve, we have used the scaling factor $f_{\rm x} = 0.0004$, penetration factor $\beta = 1.3$, black hole mass ratio $q = 0.08$, and SMBHB orbital period $T_{\rm b} = 150\,{\rm days}$ or semi-major axis $a_{\rm b} \simeq 0.59\,{\rm mpc} \simeq 620 r_{\rm g}$. Our results suggest that if the mass of the SMBH in SDSS J1201+30 is indeed about $10^7 M_\odot$, as preferred by the observations (S2012), the orbit of the SMBHB system should be elliptical with moderate eccentricity $e_{\rm b} \sim 0.3$.

4. Discussion

4.1. SMBHB model and alternatives

Several candidate small-separation SMBHBs have emerged in recent years. They are not spatially resolved, but the SMBHBs' presence has been indirectly inferred from semi-periodicities in light curves or structures in radio jets (see Section 1 for the observational evidence for SMBHBs; see also Komossa (2006) for a complete review).

We have shown that the presence of a SMBHB can naturally explain the characteristics of the light curve of the TDE in SDSS J1201+30, based on models of LLC09. In fact, other

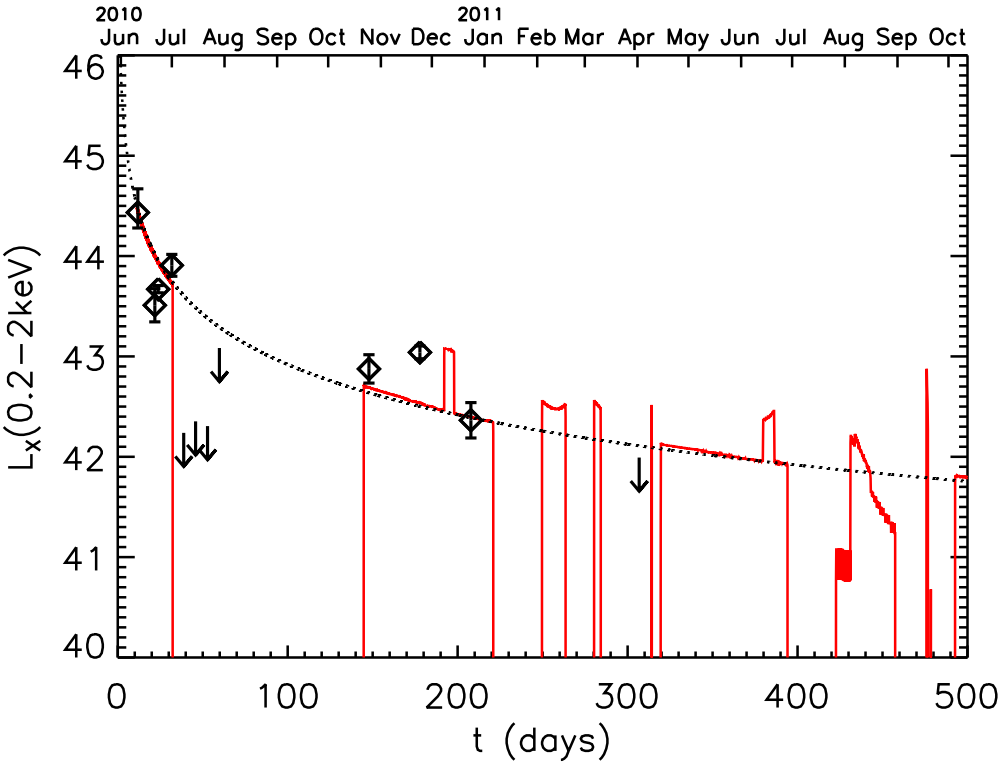

Fig. 2.— Simulated light curve in the observer frame for SDSS J1201+30 obtained with $M_{\rm BH} = 10^7 M_\odot$ and eccentricity $e_{\rm b} = 0.3$. The top x-axis gives the observation dates. The model parameters include $l = 2$, $\theta = 0.3\pi$, $\Omega = 0.2\pi$, $\omega = 1.5\pi$, $\beta = 1.3$, $q = 0.08$, $T_{\rm b} = 150\,{\rm days}$, and $\phi_{\rm b} = 1.5\pi$. The observed data from S2012 (open diamonds and arrows for upper limits) and a $t^{-5/3}$ power-law (dotted line) are overplotted.

possible explanations that might at first glance come to mind, do not well reproduce the features of the light curve, or the overall multi-wavelength properties of SDSSJ1201+30. We comment on each of them in turn.

4.1.1. Jetted TDEs, and a comparison with SwiftJ1644+57

Rapid, short-timescale variability has been detected in the light curve of the TDE candidates Swift J1644+57 (e.g., Burrows et al. 2011; Bloom et al. 2011) and Swift J2058+0516 (Cenko et al. 2012). However, unlike SDSS J1201+30, which has no detectable radio emission, both Swift J1644+57 and Swift J2058+0516 are accompanied by strong radio emission, and their isotropic X-ray luminosity, up to a few times 10^{47-48}erg s^{-1}, is well above the Eddington limit. Therefore, beaming has been suggested to explain these events (e.g., Burrows et al. 2011; Bloom et al. 2011; Levan et al. 2011; Zauderer et al. 2011). In particular, it has been suggested that the rapid dips of the X-ray light curve of Swift J1644+57 are linked to the presence of a jet, and are due to jet precession/nutation (e.g., Saxton et al. 2012a), or wobbling (Tchekhovskoy et al. 2014). Since no radio jet was detected in SDSS J1201+30, it is highly unlikely that similar scenarios are at work in this source.

4.1.2. Temporary absorption due to blobs in the accretion disk, or stellar streams, or an expanding disk wind

If an optically thick blob in the accretion disk extends vertically above a slim disk and crosses the line-of-sight (l.o.s; the disk is always optically thick in the radial direction for the slim or standard thin disk in which we are interested), the absorption by the blob may lead to a sharp drop in the flux. Because the largest Keplerian period at $r_{\rm d}$ is about 7.8 hr and independent of the black hole mass, the blob should be extended to be an annulus in the phi-direction, if the entire duration of the interruption period of at least a few days is due to the eclipse. Such an annulus should be also extended in the radial direction to the entire disk, in order for the eclipse time to last about 21 days, at least 10–100 times the disk viscous timescale (cf. Equation (16)). Therefore, in this scenario, the disk must be a spherical accretion flow instead of a slim accretion disk. This is very unlikely because of the conservation of angular momentum.

A blob with radius $r_{\rm b} \geq r_{\rm d}$ in the stellar streams may completely shield the accretion disk if it crosses the l.o.s. by chance with a probability $P \sim 6 \times 10^{-4} \beta^{-3/2} M_6^{-1/2} m_*^{1/2}$. If the blob is a fraction λ of the star and not bound by self-gravity, it expands following the ejection

of unbound plasma from the system with volume $V(t) \approx 4\pi r_b^3/3 \approx \lambda^3 R_*^3 \zeta^3$, where $\zeta = (t-t_{\rm D})/t_{\rm e}$ is the expansion parameter and $t_{\rm e} \approx 1120\,{\rm s}\,\beta^{-4/3} m_*^{-1/2} r_*^{3/2}$ (Kasen & Ramirez-Ruiz 2010). At the last detection of 2010 June 30, $\Delta t = t - t_{\rm D} \simeq 27.7\,{\rm days}$ in the object rest frame suggests an expansion parameter $\zeta \approx 2137$, or a blob with expanded size $r_{\rm b} \approx 6.6\beta\lambda M_6^{-1/3} m_*^{1/3} r_{\rm d}$. For a blob with $\lambda \sim 1$, the blob is large enough to fully shield the tidal accretion disk and also still optically thick because of Thomson scattering in ionized hydrogen for an expansion parameter $\zeta \simeq 2000$ (Kasen & Ramirez-Ruiz 2010), although the probability of totally shielding the accretion disk is only $P \sim 8 \times 10^{-5} \lambda^2 \beta M_6^{-1/2} m_*^{1/2}$. However, the timescale for the blob to cross and totally shield the accretion disk is $\Delta t_{\rm ec} \sim 11\,{\rm days}\beta^{1/2} M_6^{-1/6} m_*^{1/6} \left(\frac{\Delta t}{27.7\,{\rm days}}\right)$ in the object rest frame or 13 days in the observer frame, which is about twice the observed upper limit to the timescale of absence, $\leq 7\,{\rm days}$. Recent numerical simulations suggested that for $\beta < 3$ the unbound stellar debris from the TDE remains self-gravitating and recollapses into thin streams (Guillochon et al. 2014). Therefore, the expansion parameter ζ is < 1 and any blob in the stream is unable to fully shield the tidal accretion disk to form the extremely large dip in the light curve.

If an optically thick inhomogeneous clumpy structure in an expanding, optically thin accretion-disk wind could form due to some unknown reason after the accretion has passed the peak accretion rate for some time, it may completely absorb the disk emission and form the dips. However, to fully cover the accretion disk, the clumpy structure must extend to as large as the accretion disk or the clumpy structure in the disk wind is global. Because the clump is optically thick and would radiate at the order of the Eddington luminosity with a temperature about 10^5 K before it becomes optically thin (Strubbe & Quataert 2009), it would emit a peak radiation at the UV and soft-X-ray bands and should have been detected with *XMM*.

4.1.3. Transient eclipses due to stars or an optically-thick dense molecular cloud infalling toward the central SMBHs

A giant star or a dense optically thick gas cloud infalling toward the central SMBHs with extent along the orbital plane $\Delta R \geq (21/7) 2 r_{\rm d} \approx 6 r_{\rm d}$ may transit and completely shield the accretion disk to form a full eclipse within seven days of 21 day duration, as was suggested for some AGNs (e.g., McKernan & Yaqoob 1998; Gillessen et al. 2012; Béky & Kocsis 2013). For a giant star with radius $R_* \simeq 100 R_\odot$, it requires a SMBH mass $M_{\rm BH} \leq 4.6 \times 10^3 M_\odot (\beta/2)^3 r_*^{-3} m_*$ in order for the giant star to completely shield the accretion disk. For a falling dense gas cloud to cross the tidal accretion disk and form a total eclipse within $7/(1+z)$ days, the dense gas cloud should be at a distance from the central SMBH

$r_{\rm gas} \lesssim 1.6\times10^5 r_{\rm g}\beta^2(\frac{\Delta t}{6\,{\rm days}})^2 M_6^{-2/3} r_*^{-2} m_*^{2/3}$ and have an extension along the orbital plane $\Delta R_\parallel > 6r_{\rm d}$ and vertical to the orbital plane $\Delta R_\perp > 2r_{\rm d}$. The dense gas cloud would subtend a solid angle toward the SMBH $\Delta\Omega \gtrsim \Delta R_\parallel \Delta R_\perp / r_{\rm gas}^2 \approx 1.1\times10^{-6}\beta^{-6} r_*^6 m_*^{-2}(\frac{\Delta t}{6\,{\rm days}})^{-4}$, implying a probability $P \gtrsim 9\times10^{-8}$ for such a dense gas cloud to cross the l.o.s. by chance. The probability can increase significantly if the dense cloud has much larger size or the galactic nucleus is full of small dense clouds similar to those in the broad-line regions of AGNs. In both cases, the gas clouds should be ionized by the tidal flare and emit strong broad emission lines. However, these have not been detected in the optical spectra taken at 12 days and 11 months after the discovery of the TDE (S2012).

4.1.4. Blobby accretion near last stable orbit or other AGN-like variability

In rare cases, AGN light curves do show occasional rapid drops or flares by factors of a few or more. Therefore, whatever causes short-time variability in AGN accretion disks could potentially also be at work in any TDE source, like in SDSS J1201+30. However, it is clear that accretion disks in AGNs and tidal disruption events are significantly different: the accretion disk in AGNs can extend outward to several thousands of Schwarzschild radii or more, but the size of the accretion disk in TDEs can only be as large as a few dozens of Schwarzschild radii (i.e., hundreds of times smaller). Therefore, the characteristic timescales of the sources driving the variations in AGNs (Kelly et al. 2009, 2011; Tanaka & Menou 2010) range from a few hours up to a few hundreds of years for AGNs, but are always less than the viscous timescale $2.8\,{\rm hr}\,\alpha_{-1}^{-1}(\beta/2)^{-3/2}$ in TDEs (e.g., De Colle et al. 2012). The observational timescale of order of days for SDSS J1201+30 is much larger than the characteristic timescales of the driving sources in TDEs, which suggests stochastic variations driven by blobs or white noises superimposing on the mean luminosity as in AGNs (Kelly et al. 2009, 2011; Tanaka & Menou 2010), or in the tidal disruption event *Swift 1644+57* (De Colle et al. 2012). If the fractional amplitude of the driving noises is consistent with the observations of SDSS J1201+30 from 2010 June 10 to June 28 and between 2010 October 24 and December 23, the probability that one can detect the consecutive three observations at the extreme quiescent state of the flare from 2010 July 7 to July 21 is $P \sim p_q^3 \lesssim 10^{-15}$, where $p_q < 10^{-5}$ is the probability to observe a variability with larger than 5σ standard errors. If such large random variability with a timescale less than a few thousand seconds did exist in the light curve of SDSS J1201+30, it must have already been detected in the *XMM-Newton* pointed observations with the exposure time ranging from 10 ks to 30 ks on 2010 June 22, November 23, and December 23, which, however, was not (S2012).

4.1.5. Lense-Thirring precession of an accretion disk misaligned with a spinning SMBH

If the central SMBH is spinning and the accretion disk is misaligned with the spin axis, the disk may precess about the total angular momentum of the black hole accretion disk system as a solid body due to the Lense-Thirring torque (Fragile et al. 2007). The precession of the accretion disk would lead to quasi periodic oscillations in TDE light curves (Dexter & Fragile 2011; Stone & Loeb 2012a; Shen & Matzner 2013) and to a reduction of the observed flux up to about 50 times if the disk precesses from a face-on into edge-on phases (Ulmer 1999). For an accretion disk with surface density given by the Equation (19), the precession period is

$$T_{\rm prec} \simeq \frac{8\pi G M_{\rm BH}(1+2n)}{ac^3(5-2n)} \frac{(r_{\rm d}/r_{\rm g})^{5/2-n}\,(r_{\rm in}/r_{\rm g})^{1/2+n}\left(1-(r_{\rm in}/r_{\rm d})^{5/2-n}\right)}{1-(r_{\rm in}/r_{\rm d})^{1/2+n}} \tag{23}$$

(Fragile et al. 2007; Stone & Loeb 2012a; Shen & Matzner 2013), where a is the dimensionless black hole spin parameter with $0 \leq a < 1$. For a black hole mass $M_{\rm BH} = 10^7 M_\odot$ and typical disk parameters $n = 1/2$, $r_{\rm in} \simeq 3r_{\rm g}$, and $r_{\rm d} \simeq 2r_{\rm t} \simeq 10r_{\rm g}$, the typical disk precession period is $T_{\rm prec} \approx 2.84\,{\rm days}\,a^{-1}M_7$, or in the observer frame, $T_{\rm prec,obs} = (1+z)T_{\rm prec} \approx 3.25\,{\rm days}\,a^{-1}M_7 \gtrsim 3.25\,{\rm days}\,M_7$. While for a black hole mass $M_{\rm BH} = 10^6 M_\odot$ and typical disk parameters $n = 1/2$, $r_{\rm in} \simeq 3r_{\rm g}$, and $r_{\rm d} \simeq 2r_{\rm t} \simeq 47r_{\rm g}$, the typical precession period is $T_{\rm prec} \approx 5.2\,{\rm days}\,a^{-1}M_6$, or in the observer frame, $T_{\rm prec,obs} = (1+z)T_{\rm prec} \approx 5.9\,{\rm days}\,a^{-1}M_6$. If the large drop in the light curve of SDSS J1201+30 is due to the disk Lense-Thirring precession with period $T_{\rm prec,obs} \gtrsim 3.25\,{\rm days}\,M_7$, the observations with regular time intervals of 10 days between 2010 June 10 and June 30, and 7 days between 2010 July 7 and July 28 of S2012 suggest that the face- and edge-on phases should be, respectively, longer than 20 days and 21 days. Therefore, the observations obtained between 2010 June 10 and July 28 imply that the precession period should have $T_{\rm prec,obs} \geq 48\,{\rm days}$. However, the observations of the TDE between 2010 October 24 and December 23 suggest a face-on phase longer than 60 days and thus a precession period $T_{\rm prec,obs} \gtrsim 81\,{\rm days}$. The observation of 2010 December 23 suggests $T_{\rm prec,obs} \geq 84.5\,{\rm days}$, while the observation of 2010 October 24 indicates $T_{\rm prec,obs} < 88\,{\rm days}$. In conclusion, if the large drop in the flux was due to the disk Lense-Thirring precession, the precession period would be $84.5\,{\rm days} < T_{\rm prec,obs} < 88\,{\rm days}$. The drop in flux by a factor 50 within seven days, or $\lesssim 8\%$ of the precession period, is too steep to be consistent with the predictions of Lense-Thirring precession (Dexter & Fragile 2011; Stone & Loeb 2012a; Shen & Matzner 2013).

4.2. Orbital parameters of the SMBHB system

All of our results were obtained with ΔE given by Equation (12) with $l = 2$. However, some numerical simulations (e.g., Stone et al. 2013; Guillochon & Ramirez-Ruiz 2013) suggest a weaker dependence of ΔE on β. To investigate the dependence of our results on the different relationships of ΔE and β, we have carried out test numerical scattering experiments with $l = 0$.

The test numerical simulations are only carried out for $M_{\rm BH} = 10^6 M_\odot$, because the present results obtained with $\Delta E \propto \beta^2$ show a large variation of β with $1.2 \lesssim \beta \lesssim 5$ for $M_{\rm BH} = 10^6 M_\odot$ but nearly a constant β with $1.3 \lesssim \beta \lesssim 1.6$ for $M_{\rm BH} = 10^7 M_\odot$. Similar to Figure 1, our results show that the simulated light curves for SDSS J1201+30 and the obtained model parameters of the star and SMBHB systems are nearly the same as those obtained with $l = 2$, which can be understood as follow: different relationships of ΔE and β significantly change only $t_{\rm min}$, which is degenerate with the scaling free parameter $f_{\rm x}$ as discussed in Section 2. Meanwhile, although ΔE is independent of β for $l = 0$, the truncation and recurrence of the light curve sensitively depends on β. Therefore, we will not discuss the results obtained with $l = 0$ any further.

We have shown that the peculiar characteristics of the light curves of the TDE in SDSS J1201+30 can be naturally explained by the SMBHB model given by LLC09. In the SMBHB model, the orbital parameters of the disrupted star approaching with negligible initial total energy can be determined to be $\theta \sim 0.3\pi$, $\Omega \sim 0.2\pi$, and $\omega \sim 1.5\pi$ independent of the detailed choices of the model parameters. By fully reproducing the X-ray light curve of the TDE with the model light curves of a SMBHB system, we have obtained that the orbit of the SMBHB in SDSS J1201+30 should be elliptical with moderate eccentricity $e_{\rm b} \simeq 0.3$ (with $0.1 \lesssim e_{\rm b} \lesssim 0.5$) and typical orbital period $T_{\rm b} \simeq 150\,{\rm days}$ (with $140\,{\rm days} \lesssim T_{\rm b} \lesssim 160\,{\rm days}$) for a primary SMBH of mass $M_{\rm BH} = 10^7 M_\odot$. A SMBH with that value is preferred by observations (S2012). The orbital period of the SMBHB suggests a semi-major axis $a_{\rm b} \simeq 0.59\,{\rm mpc} \simeq 620 r_{\rm g}$. The black hole mass ratio, the penetration factor of that star, and the initial orbital phase at disruption have typical values $q \simeq 0.08$, $\beta \simeq 1.3$, and $\phi_{\rm b} \simeq 1.5\pi$, respectively. Because the parameters q, $e_{\rm b}$, and β are three important model quantities and the simulation results sensitively depend on their values, we have carried out a large amount of simulations in three-dimensional space. The results are given in the panels (a)-(l) of Figure 3. In the simulations, we have adopted $\phi_{\rm b} = 1.5\pi$ for simplicity. The simulation results show that the model solutions to the X-ray light curve of the TDE consist only of a small domain in the four-dimensional space (β, q, $e_{\rm b}$, $T_{\rm b}$) with $T_{\rm b} \sim 150\,{\rm days}$. In panels (a)-(b) of Figure 3, we show the results obtained with $T_{\rm b} = 140\,{\rm days}$ only for $e_{\rm b} = 0.1$ and 0.2, and $0.03 \leq q \leq 0.2$, although we have done simulations for $0.1 \leq e_{\rm b} \leq 0.9$ and

$0.03 \leq q \leq 0.9$, because no model light curve obtained with parameters outside the ranges can reproduce the X-ray light curve of the TDE. In panels (c)-(l), we show the simulation results in the three-dimensional space (β, q, $e_{\rm b}$) for $T_{\rm b} = 145, 150, 155, 160$ days. Because the model solutions are insensitive to the small change of the orbital period, we have only done the simulations for $0.1 \leq e_{\rm b} \leq 0.6$, $1.2 \leq \beta \leq 1.6$, and $0.03 \leq q \leq 0.09$.

However, the mass of the central black hole can be smaller. If the SMBH has a mass $M_{\rm BH} = 10^6 M_\odot$, we have shown that the X-ray light curve of the TDE can also be reproduced with the model light curves obtained with SMBHB systems of orbits either circular $e_{\rm b} = 0$ or elliptical $e_{\rm b} \lesssim 0.5$. The fitted orbital period of the SMBHB depends weakly on the orbital eccentricities and has a typical value of $T_{\rm b} \simeq 140$ days (or $a_{\rm b} \simeq 0.26$ mpc) with 132 days $\lesssim T_{\rm b} \lesssim 145$ days if $e_{\rm b} = 0$ or $T_{\rm b} \simeq 150$ days (or $a_{\rm b} \simeq 0.28$ mpc) with 142 days $\lesssim T_{\rm b} \lesssim 156$ days if $e_{\rm b} = 0.2$. The fitted mass ratio of the SMBHB system in SDSS J1201+30 has a typical value $q \sim 0.1$ for any possible orbit with $e_{\rm b} \lesssim 0.5$, but distributes in a range depending sensitively on the values of eccentricity and penetration factor. The panels from (m) to (r) of Figure 3 show the complex dependence among q, $e_{\rm b}$, and β in the parameter space, which are adopted from our simulation results for $0 \leq e_{\rm b} \leq 0.9$ and $0.03 \leq q \leq 0.9$. In the simulations, we have taken $T_{\rm b} = 140$ days for $e_{\rm b} = 0$ and $T_{\rm b} = 150$ days and $\phi_{\rm b} = 1.7\pi$ for $e_{\rm b} > 0$ for simplicity. Different orbital periods are adopted here for different types of orbits in order to give the largest domain of model solutions in the parameter space. Again, the results depend only weakly on the orbital periods, in the sense that the variation of the orbital period in a certain range only changes the boundaries, but not the shape of the domain of the model solutions in the parameter space.

The model solutions of the observed X-ray light curve are obtained with the assumption that the disrupted star is a solar-type main-sequence star. The disrupted star may be a different type of star, with different internal structures, masses, and/or radii. The tidal disruption of stars with different internal structures would lead to different light curves with different peak luminosities, peak time $t_{\rm peak}$, and power-law indices other than $-5/3$ (Lodato et al. 2009; Guillochon & Ramirez-Ruiz 2013). Because the key features of the interruptions and recurrences in the model light curves do not change with the structure of the star, our conclusions regarding the model solutions and the parameters are robust. For a certain orbital pericenter, Equation (12) suggests the maximum specific energy ΔE changes with the radius of the star. The differences in ΔE do not change our conclusions as discussed before. However, our results do sensitively depend on the orbital pericenter $r_{\rm p}$ or β for a certain tidal radius $r_{\rm t}$. If we have the knowledge of the star, with the condition $r_{\rm p} \leq r_{\rm t}$ or from Equation (10) we may give some more strict constraints on $r_{\rm p}$ (or β) and thus the mass ratio q (and probably $e_{\rm b}$), based on Figure 3. Notice that in Figure 3 $\beta = \beta_\odot \equiv r_{\rm t,\odot}/r_{\rm p}$ with $r_{\rm t,\odot}$ the tidal radius of a solar-type star.

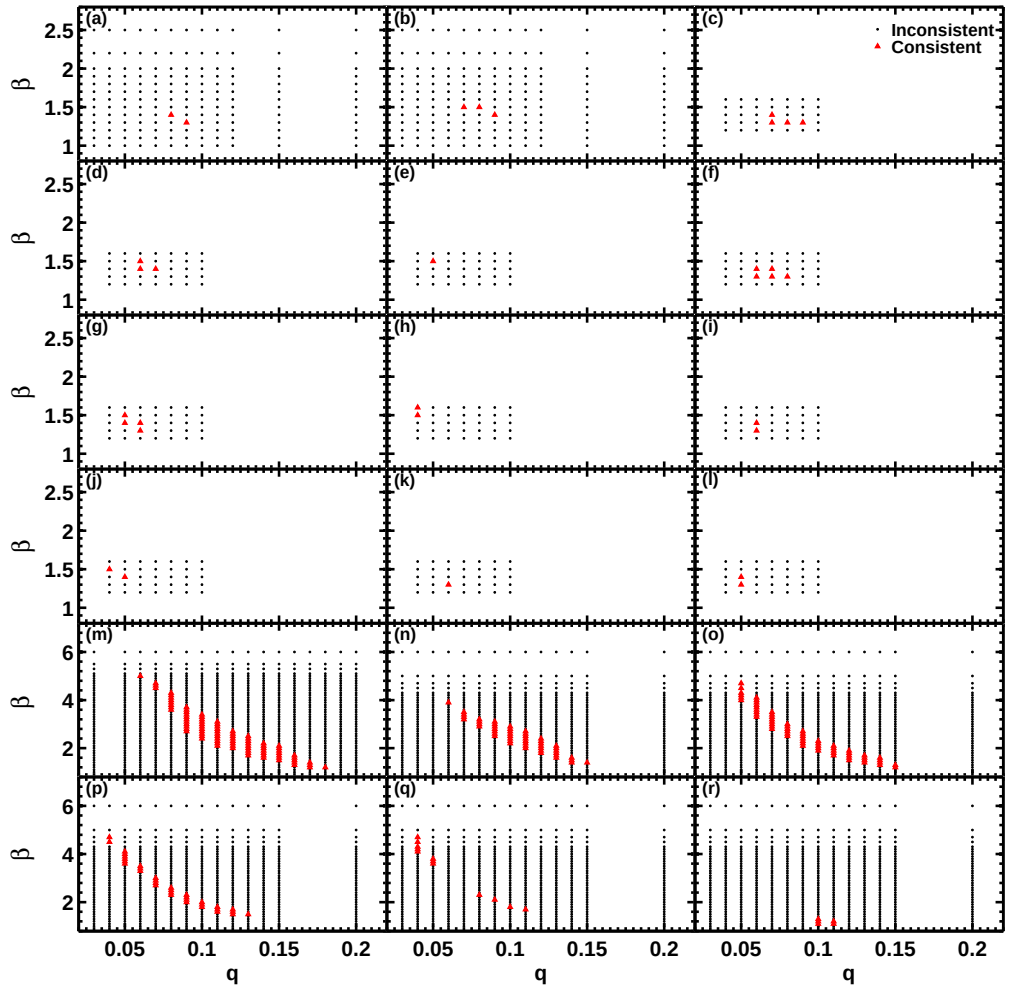

Fig. 3.— Simulation results for the TDE of SDSS J1201+30 in the ($e_{\rm b}$, q, β) space for which the model light curves have been simulated. Numerical simulations have been done in the ($e_{\rm b}$, q, and β) space with $0 \leq e_{\rm b} \leq 0.9$, $0.03 \leq q \leq 0.9$, and $1 \leq \beta \leq 6$ for $M_{\rm BH} = 10^6 M_\odot$ or $1 \leq \beta \leq 2.5$ for $M_{\rm BH} = 10^7 M_\odot$. For ellipticity, those values, for which no model light curve is consistent with the observations of the TDE, are not shown here. In the computed domain of the parameter spaces, the fraction marked with the red triangle can give model light curves consistent with the observations of the TDE, while the other (marked with black dots) cannot. Panels (a)-(l) are results for $M_{\rm BH} = 10^7 M_\odot$ with $\phi_{\rm b} = 1.5\pi$: panels (a)-(b) for $e_{\rm b} = 0.1$ and 0.2 with $T_{\rm b} = 140$ days; panels (c)-(e) for $e_{\rm b} = 0.2$, 0.3, and 0.4 with $T_{\rm b} = 145$ days; panels (f)-(h) for $e_{\rm b} = 0.3$, 0.4, and 0.5 with $T_{\rm b} = 150$ days; panels (i)-(j) for $e_{\rm b} = 0.4$ and 0.5 with $T_{\rm b} = 155$ days; panels (k)-(l) for $e_{\rm b} = 0.4$ and 0.5 with $T_{\rm b} = 160$ days. Panels (m)-(r) are for $M_{\rm BH} = 10^6 M_\odot$ and $e_{\rm b} = 0, 0.1, 0.2, 0.3, 0.4$, and 0.5, respectively. In the simulations, $T_{\rm b} = 140$ days for $e_{\rm b} = 0$ or $T_{\rm b} = 150$ days and $\phi_{\rm b} = 1.7\pi$ for $e_{\rm b} \geq 0.1$ are adopted.

We have carried out numerical simulations to scan a significant fraction of the large model parameter space, but it is still prohibitive for the present computing powers to cover the whole space of the parameters (θ, Ω, ω, β, $T_{\rm b}$, q, $e_{\rm b}$, and $M_{\rm BH}$). From the first principles, the potential sphere of the restricted three-body systems consisting of the SMBHB and the stellar plasma elements is split into inner and outer regions by the SMBHB orbit. As argued for Newtonian potential analytically by Mardling (2007) and numerically by LLC09, the shell of the potential sphere centered on the SMBHB orbit is chaotic because of the nonlinear overlap of the multiple resonances due to the strong perturbations by the secondary SMBH. The fluid elements with orbits inside the chaotic shell regions are resonantly scattered off and thus the inner and outer boundaries of the chaotic shell regions determine, respectively, the interruption and recurrence time of the TDE light curve. For a circular SMBHB orbit, the orbit of the SMBHB binary roughly determines the centers of the chaotic regions, suggesting that the Keplerian orbital period of the SMBHB is roughly between the time of the interruption and recurrence. The BH mass ratio determines the strength of the resonant perturbation, the extent of the nonlinear overlap of multiple resonances, and how effectively the fluid elements with orbits inside or crossing the chaotic shell regions are scattered off on the timescale when they move inside the chaotic shell, deciding the duration and shapes (e.g., smooth or flickering) of the interruptions and the recurrent light curves. The orbital parameters of the star could modify the characteristics of the key features of the SMBHB system only moderately. The high-quality X-ray light curve obtained by S2012 did not only catch the time of the interruption, the recurrence, and the re-interruption of the TDE, but also constrains well the long durations of the phases of low and high flux. The long duration of the recurrence suggests that the resonant perturbation by the secondary BH should not be too strong and the merger should not be a major merger with $q \gtrsim 0.3$, while the long duration of the interruption implies that the perturbation cannot be too weak and the merger should not have an extreme mass ratio $q \lesssim 0.01$ irrespective to the detailed modeling of the light curve. Therefore, the solutions with $q \sim 0.08$ are certain. With a moderate small mass ratio $q \sim 0.08$, the duration of the recurrent flare should not be much longer than the observed one, suggesting that the time of recurrence should not be much earlier than the first detection of the recurrent flare and the SMBHB orbital period is about the time of recurrence. Therefore, the model solutions with $T_{\rm b} \sim 150\,{\rm days}$ are robust, too. However, we have to notice that the orbital period of the SMBHB is the Keplerian period, but the return time of the bound stellar plasma elements is determined by the radial epicyclic frequency. The Keplerian and epicyclic frequencies are equal in Newtonian gravity, but the latter is smaller than the former in GR. The differences between the two frequencies become significant for tidal disruptions by the SMBH with $M_{\rm BH} \gtrsim 10^7 M_\odot$ because the tidal radius for a solar-type star is $r_{\rm t} \lesssim 5 r_{\rm g} M_7^{-2/3}$. Therefore, for the certain orbital period $T_{\rm b}$, the time of the interruption in the model light curves is delayed so much that it is significantly later

than the date of the first upper limit, which, for a SMBHB system with circular orbit, is hardly compensated by adjusting the other parameters. To significantly shift the time of interruption to an earlier date, we need an elliptical orbit for the SMBHB system. For the SMBHB system with the given orbital period, the moderate eccentricity decreases significantly the pericenter and thus the inner boundary of the chaotic shell region, resulting in the appearance of the interruption before the first upper limit on 2010 July 7 and after the last detection on 2010 June 30. Therefore, we expect that the solution for $M_{\rm BH} = 10^7 M_\odot$ with $e_{\rm b} \sim 0.3$ is robust.

4.3. Gravitational wave emission

Upon final coalescence, SMBHB systems like the one in SDSS J1201+30 are prime sources for future space-based GW missions like *eLISA*. However, in its current state of evolution, it would be challenging to detect the GWs from this system. It would radiate GW emission at a frequency $f_{\rm obs} = 2/T_{\rm b}(1+z) \simeq 0.13\,\mu{\rm Hz}\,(T_{\rm b}/150\,{\rm days})^{-1}$ in the observer frame, and with a characteristic strain in an observation of duration $\tau_{\rm obs}$

$$h_{\rm c} = h_{\rm r}\sqrt{f_{\rm obs}\tau_{\rm obs}}, \tag{24}$$

with $h_{\rm r}$ is the strain amplitude at the object rest frequency, $f_{\rm b} = 2/T_{\rm b}$

$$h_{\rm r} = \frac{8\pi^{2/3}}{10^{1/2}}\frac{G^{5/3}M^{5/3}}{c^4 r(z)} f_{\rm b}^{2/3}, \tag{25}$$

where $M = (M_1M_2)^{3/5}/(M_1+M_2)^{1/5} = M_{\rm BH}q^{3/5}/(1+q)^{1/5}$ is the "chirp mass" of the SMBHB and $r(z)$ is the comoving distance. The frequency $f_{\rm obs} \simeq 0.13\,\mu$Hz is in the range observable with PTAs, but much smaller than that of *eLISA*. For a five-year PTA observation, the expected characteristic strain of the binary is

$$\begin{aligned} h_{\rm c} &\approx 1.7\times10^{-20}\left(\frac{T_{\rm b}}{140\,{\rm days}}\right)^{-7/6}\left(\frac{\tau_{\rm obs}}{5\,{\rm yr}}\right)^{1/2} M_6^{5/3}\frac{q_{-1}}{(1+q)^{1/3}} \\ &\approx 6.0\times10^{-19}\left(\frac{T_{\rm b}}{150\,{\rm days}}\right)^{-7/6}\left(\frac{\tau_{\rm obs}}{5\,{\rm yr}}\right)^{1/2} M_7^{5/3}\frac{(q/0.08)}{(1+q)^{1/3}}, \end{aligned} \tag{26}$$

which is about four orders of magnitude smaller than the detection limit of PTA at the frequency $f_{\rm obs}$ (e.g., Ellis et al. 2012). If GW radiation was the only contribution to the orbital shrinkage, the lifetime of the system is

$$\tau_{\rm gw} \simeq 1.0\times10^8\,{\rm yr}\left(\frac{T_{\rm b}}{140\,{\rm days}}\right)^{8/3} M_6^{-5/3}q_{-1}^{-1}f^{-1}(1+q)^{1/3} \tag{27}$$

(Peters & Mathews 1963), where f is a function of the eccentricity $e_{\rm b}$

$$f = \left(1 + \frac{73}{24}e_{\rm b}^2 + \frac{37}{96}e_{\rm b}^4\right)\left(1 - e_{\rm b}^2\right)^{-7/2}. \quad (28)$$

For a SMBHB system with $M_{\rm BH} = 10^7 M_\odot$ and typical parameter values $T_{\rm b} = 150\,{\rm days}$, $q = 0.08$, and $e_{\rm b} = 0.3$, the life time is $\tau_{\rm gw} \simeq 1.9 \times 10^6\,{\rm yr}$, while for a SMBHB system with $M_{\rm BH} = 10^6 M_\odot$ and the parameter values $T_{\rm b} = 140\,{\rm days}$, $q = 0.1$ and $e_{\rm b} = 0$, the life time is longer, with $\tau_{\rm gw} \simeq 1.0 \times 10^8\,{\rm yr}$. However, a longer life time $\tau_{\rm gw}$ does not necessarily imply that the $10^6 M_\odot$ fit is favored, nor that TDE light curve searches for SMBHBs are biased toward systems with larger separations and smaller SMBH masses for a given observed binary period. This is because of the biases in event detection in any (X-ray, transient) survey, which preferentially selects for the most luminous, most frequent events. In particular, X-ray surveys are biased toward SMBHs of higher mass $M_{\rm BH} \approx 10^7 M_\odot$ because of their higher peak luminosities. Further, the TDE rate $N_{\rm TDE}$ is a function of $a_{\rm b}$. A preliminary estimation suggests that $N_{\rm TDE}$ is a complicated function of $a_{\rm b}$ and does not change significantly for $10^{-3}\,{\rm pc} \lesssim a_{\rm b} \lesssim 1\,{\rm pc}$ (Chen et al. 2011; Liu & Chen 2013). Thus, for a given observed $T_{\rm b}$ in an X-ray transient survey, a SMBHB system with higher SMBH mass $M_{\rm BH} \sim 10^7 M_\odot$ and smaller separation within the range of $10^{-3}\,{\rm pc} \lesssim a_{\rm b} \lesssim 1\,{\rm pc}$ would be likely favored.

4.4. Frequency of SMBHBs among known TDEs

Approximately 20 to 25 TDEs and candidates have been identified from the observations (see Komossa 2012, for a recent review), including the X-rays (e.g., Komossa & Bade 1999), UV (Gezari et al. 2008), optical and emission lines (Komossa et al. 2008b; van Velzen et al. 2011), and gamma-rays (e.g., Burrows et al. 2011; Bloom et al. 2011; Cenko et al. 2012). We have inspected these light curves, with the exception of the two jetted TDEs, in order to search for similar features as seen in SDSSJ1201+30. None are clearly present. This might have several reasons. It could be due to the gaps in the light curves of the TDEs (and so escaped detection). Alternatively, the orbital timescales of the SMBHBs can be longer or shorter, and so their effects would be undetectable on the timescales observed so far. Currently, this then makes SDSS J1201+30 the only good SMBHB candidate among the known TDEs.

In summary, we conclude that the SMBHB model for SDSS J1201+30 is a viable model that naturally explains the abrupt dips and recoveries of the X-ray light curve of the event. Future sky surveys are expected to detect TDEs in the thousands. Analysis of their light curves will then provide a powerful new tool of searching for SMBHBs in otherwise non-active galaxies.

We are grateful to Peter Berczik, Xian Chen, Zoltan Haiman, Luis Ho, Richard Saxton, Rainer Spurzem, and Takamitsu Tanaka for helpful discussions. We would like to thank the anonymous referee for the very useful comments and suggestions. This work is supported by the National Natural Science Foundation of China (NSFC11073002 and NSFC11303039). F.K.L. thanks the open funding (No. Y3KF281CJ1) from Key Laboratory of Frontiers in Theoretical Physics, Institute of Theoretical Physics, of CAS for financial support. S.L. acknowledges support by NAOC CAS through the Silk Road Project (grant No. 2009S1-5 for R. Spurzem) and the "Qianren" (Thousand Talents Plan) Project for R. Spurzem. S.K. would like to thank the Kavli Institute for Theoretical Physics (KITP) for their hospitality and support during the program on "A universe of black holes." This research was supported in part by the National Science Foundation under grant No. NSF PHY11-25915. The computations have been done on the Laohu supercomputer at the Center of Information and Computing at National Astronomical Observatories, Chinese Academy of Sciences, funded by Ministry of Finance of People's Republic of China under the grant $ZDYZ2008-2$.

REFERENCES

Abramowicz, M.A., Czerny, B., Lasota, J.P., & Szuszkiewicz, E. 1988, ApJ, 332, 646

Armitage, P.J., & Natarajan, P. 2005, ApJ, 634, 921

Begelman, M. C., Blandford, R. D., & Rees, M. J. 1980, Nature, 287, 307

Béky, B., & Kocsis, B. 2013, ApJ, 762, 35

Berczik, P., Merritt, D., Spurzem, R., & Bischof, H.-P. 2006, ApJ, 642, L21

Bloom, J.S., Giannios, D., Metzger, B.D., et al. 2011, Sci, 333, 203

Britzen, S., Zamaninasab, M., Aller, M., et al. 2012, JPhCS, 372, 012029

Burrows, D.N., Kennea, J.A., Ghisellini, G., et al. 2011, Nature, 476, 421

Cappelluti, N., Ajello, M., Rebusco, P., et al. 2009, A&A, 495, L9

Cenko, S.B., Krimm, H.A., Horesh, A., et al. 2012, ApJ, 753, 77

Chen, X., & Liu, F. K. 2013, ApJ, 762, 95

Chen, X., Liu, F. K., & Magorrian, J. 2008, ApJ, 676, 54

Chen, X., Madau, P., Sesana, A., & Liu, F. K. 2009, ApJ, 697, L149

Chen, X., Sesana, A., Madau, P., & Liu, F. K. 2011, ApJ, 729, 13

Civano, F., Elvis, M., Lanzuisi, G., et al. 2012, ApJ, 752, 49

Colpi, M. & Dotti, M., 2011, ASL, 4, 181

Conway, J.E., & Wrobel, J.M. 1995, ApJ, 439, 98

De Colle, F., Guillochon, J., Naiman, J., & Ramirez-Ruiz, E. 2012, ApJ, 760, 103

Dexter, J., & Fragile, P.C. 2011, ApJ, 730, 36

Donato, D., Cenko, S.B., Covino, S., et al. 2014, ApJ, 781, 59

Ellis, J.A., Siemens, X., & Creighton, J.D.E. 2012, ApJ, 756, 175

Esquej, P., Saxton, R.D., Komossa, S., et al. 2008, A&A, 489, 543

Evans, C.R., & Kochanek, C. S.; 1989, ApJ, 346, L13

Fabbiano, G., Wang, J., Elvis, M., & Risaliti, G. 2011, Nature, 477, 431

Fragile, P.C., Blaes, O.M., Anninos, P., & Salmonson, J.D. 2007, ApJ, 668, 417

Gezari, S., Basa, S., Martin, D.C., et al. 2008, ApJ, 676, 944

Gezari, S., Chornock, R., Rest, A., et al. 2012, Nature, 485, 217

Gezari, S., Heckman, T., Cenko, S.B., et al. 2009, ApJ, 698, 1367

Gillessen, S., Genzel, R., Fritz, T.K., et al. 2012, Nature, 481, 51

Gould, A., & Rix, H.-W. 2000, ApJ532, L29

Green, P.J., Myers, A.D., Barkhouse, W.A., et al. 2010, ApJ, 710, 1578

Guillochon, J., Manukian, H., & Ramirez-Ruiz, E. 2014, ApJ, 783, 23

Guillochon, J., & Ramirez-Ruiz, E. 2013, ApJ, 767, 25

Hayasaki, K., Stone, N., & Loeb, A. 2013, MNRAS, 434, 909

Hills, J. G. 1975, Nature, 254, 295

Ivanov, P.B., Polnarev, A.G., & Saha, P. 2005, MNRAS, 358, 1361

Iwasawa, M., An, S., Matsubayashi, T., Funato, Y., & Makino, J. 2011, ApJ, 731, L9

Ju, W.H., Greene, J.E., Rafikov, R.R., Bickerton, S.J., & Badenes, C. 2013, ApJ, 777, 44

Kasen, D., & Ramirez-Ruiz, E. 2010, ApJ, 714, 155

Kelly, B.C., Bechtold, J., & Siemiginowska, A. 2009, ApJ, 698, 895

Kelly, B.C., Sobolewska, M., & Siemiginowska, A. 2011, ApJ, 730, 52

Kocsis, B., Haiman, Z., & Loeb, A. 2012, MNRAS, 427, 2680

Komossa, S. 2002, RvMA, 15, 27

Komossa, S. 2006, Mem. Soc. Astron. Italiana, 77, 733

Komossa, S. 2012, EPJ Web Conf., 39, 02001

Komossa, S., & Bade, N. 1999, A&A, 343, 775

Komossa, S., Burwitz, V., Hasinger, G., et al.2003, ApJ, 528, L15

Komossa, S., Halpern, J., Schartel, N., et al. 2004, ApJ, 603, L17

Komossa, S., & Merritt, D. 2008, ApJ, 683, L21

Komossa, S., Zhou, H., & Lu, H. 2008a, ApJ, 678, L81

Komossa, S., Zhou, H., Wang, T., et al. 2008b, ApJ, 678, L13

Kozai, Y. 1962, AJ, 67, 591

Kulier, A., Ostriker, J.P., Natarajan, P., Lackner, C.N., & Cen, R. 2013, ApJ, in press (arXiv:1307.3684)

Kulkarni, G., & Loeb, A. 2012, MNRAS, 422, 1306

Levan, A.J., Tanvir, N.R., Cenko, S.B., et al. 2011, Sci, 333, 199

Li, L.-X.; Narayan, R.; & Menou, K.; 2002, ApJ, 576, 753

Li, S., Liu, F.K., Berczik, P., Chen, X., & Spurzem, R. 2012, ApJ, 748, 65

Lidov, M. L., 1962, P&SS, 9, 719

Liu, F. K. 2004, MNRAS, 347, 1357

Liu, F. K., & Chen, X. 2007, ApJ, 671, 1272

Liu, F. K., & Chen, X. 2013, ApJ, 767, 18

Liu, F. K., Li, S., & Chen, X. 2009, ApJ, 706, L133 (LLC09)

Liu, F.K., Liu, B.F., & Xie, G.Z. 1995, A&AS, 123, 569

Liu, F. K., Wang, D., & Chen, X. 2012, ApJ, 746, 176

Liu, F. K., & Wu, X.-B. 2002, A&A, 388, L48

Liu, F. K., Wu, X.-B., & Cao, S. L. 2003, MNRAS, 340, 411

Liu, F. K., Xie, G.Z., & Bai, J.M. 1995, A&A, 295, 1

Liu, F. K., Zhao, G., & Wu X.-B. 2006, ApJ, 650, 749

Liu, X., Greene, J.E., Shen, Y., & Strauss, M.A. 2010, ApJ, 715, L30

Lodato, G., King, A. R., & Pringle, J. E. 2009, MNRAS, 392, 332

Luminet, J.-P. 1985, AnPh, 10, 101

Lynden-Bell, D., & Pringle, J.E. 1974, MNRAS, 168, 603

Magorrian, J., & Tremaine, S. 1999, MNRAS, 309, 447

Maksym, W.P., Ulmer, M.P., & Eracleous, M. 2010, ApJ, 722, 1035

Mardling, R. A. 2007, in IAU Symp. 246, Dynamical Evolution of Dense Stellar Systems, ed. E. Vesperini, M. Giersz, & A. Sills (Cambridge: Cambridge Univ. Press), 199

Mardling, R. A., & Aarseth, S. J. 2001, MNRAS, 321, 398

Mayer, L., Kazantzidis, S., Madau, P., et al. 2007, Sci, 316, 1874

McKernan, B., & Yaqoob, T. 1998, ApJ, 501, L29

McWilliams, S.T., Ostriker, J.P., Pretorius, & Frans, F. 2012, Sci, submitted (arXiv:1211.4590)

Merritt, D., & Poon, M. Y. 2004, ApJ, 606, 788

Naab, T., Johansson, P.H., & Ostriker, J.P. 2009, ApJ, 699, L178

Narayan, R., & McClintock, J. E. 2012, MNRAS, 419, L69

Narayan, R., & Yi, I. 1995, ApJ, 428, L13

Paczyńsky, B., & Wiita, P. J. 1980, A&A, 88, 23

Perets, H.B., Hopman, C., & Alexander, T. 2007, ApJ, 656, 709

Peters, P.C., & Mathews, J. 1963, PhRv, 131, 435

Phinney, E. S. 1989, in IAU Symp. 136, The Center of the Galaxy, ed. M. Morris (Dordrecht: Kluwer), 543

Preto, M., Berentzen, I., Berczik, P., & Spurzem, R. 2011, ApJ, 732, L26

Qian, S.-J., Kudryavtseva, N.A., Britzen, S., et al. 2007, Chinese J. Astron. Astrophys., 7, 364

Quinlan, G.D. 1996, New A, 1, 35

Rees, M. J. 1988, Nature, 333, 523

Rodriguez, C., Taylor, G.B., Zavala, R.T., et al. 2006, ApJ, 646, 49

Roland, J., Britzen, S., Kudryavtseva, N.A., Witzel, A., & Karouzos, M. 2008, A&A, 483, 125

Saxton, C.J., Soria, R., Wu, K., & Kuin, N.P.M. 2012a, MNRAS, 422, 1625

Saxton, R.D., Read, A.M., Esquej, P., et al. 2012b, A&A, 541, A106 (S2012)

Sesana, A., Gualandris, A., & Dotti, M. 2011, MNRAS, 415, L35

Shakura, N.I., & Sunyaev, R.A. 1973, A&A, 24, 337

Shen, R.-F., & Matzner, C.D. 2013, ApJ, in press (arXiv:1305.5570)

Shen, Y., Liu, X., Loeb, A., & Tremaine, S. 2013, ApJ, 775, 49

Sillanpaa, A., Haarala, S., Valtonen, M. J., Sundelius, B., & Byrd, G. G. 1988, ApJ, 325, 628

Stone, N., & Loeb, A. 2011, MNRAS, 412, 75

Stone, N., & Loeb, A. 2012a, Phys. Rev. Lett., 108, 061302

Stone, N., & Loeb, A. 2012b, MNRAS, 422, 1933

Stone, N., Sari, R., & Loeb, A. 2013, MNRAS, 435, 1809

Strubbe, L.E., & Quataert, E. 2009, MNRAS, 400, 2070

Tanaka, T. 2011, MNRAS, 410, 1007

Tanaka, T. 2013, MNRAS, 434, 2275

Tanaka, T., & Haiman, Z. 2009, ApJ, 696, 1798

Tanaka, T., & Menou, K. 2010, ApJ, 714, 404

Tchekhovskoy, A., Metzger, B.D., Giannios, D., & Kelley, L.Z. 2014, MNRAS, 437, 2744

Tsalmantza, P., Decarli, R., Dotti, M., & Hogg, D.W. 2011, ApJ, 738, 20

Ulmer, A. 1999, ApJ, 514, 180

Valtonen, M.J., Lehto, H.J., Takalo, L.O., & Sillanpää, A. 2011, ApJ, 729, 33

van Dokkum, P.G., Whitaker, K.E., Brammer, G., et al. 2010, ApJ, 709, 1018

van Velzen, S., Farrar, G.R., Gezari, S., et al. 2011, ApJ, 741, 73

Vasiliev, E., & Merritt, D. 2013, ApJ, 774, 87

Volonteri, M., Haardt, F., & Madau, P. 2003, ApJ, 582, 559

Wang, J., & Merritt, D. 2004, ApJ, 600, 149

Wegg, C., & Nate Bode, J. 2011, ApJ, 738, L8

Zauderer, B.A., Berger, E., Soderberg, A.M., et al. 2011, Nature, 476, 425

This preprint was prepared with the AAS LaTeX macros v5.2.